minus minimum of the QTce (max-min QTce) and standard deviation of the QTce (SD-QTce) among all 87 leads was also measured.

Follow-Up

Patients were prospectively followed for a maximum of 24 months after the second ECG recording during oral amiodarone. The endpoint was recurrence of sustained VT, ventricular fibrillation (VF), or sudden cardiac death. Sustained VT was defined as a tachycardia of ventricular origin at a rate of >100 beats/min and lasting for >30 seconds or resulting in hemodynamic collapse. No patients received any antiarrhythmic drugs other than oral amiodarone during the follow-up periods. The relationship between the repolarization parameters obtained from 12- and 87-lead and subsequent arrhythmic events was investigated.

Statistical Analysis

Data are expressed as mean ± SD for continuous variables and percentage for categorical variables, and compared by the paired *t* test. Univariate predictors of arrhythmic events were evaluated using the Cox proportional hazard model. Multivariate Cox models were used to test the independence of significant factors by univariate Cox regression analysis, including clinical variables. The receiver operating characteristics (ROC) curves, which analyze the sensitivity as the function of the complement of specificity, were used to evaluate the accuracy of the repolarization parameters. Event-free curves were generated using the Kaplan-Meier method, and compared by the log-rank test. A value of $P < 0.05$ was considered statistically significant.

Results

Change of Repolarization Parameters with Chronic Amiodarone

Figure 1 illustrates superimposed 87-lead ECGs before and after amiodarone in two cases. In the first case (panel A), the max and min QTce interval after amiodarone were similar to those before amiodarone, thus the max-min QTce, SD-QTce, and mean Tcp-e were not increased after amiodarone. On the other hand, in another case (panel B), the max QTce was remarkably prolonged after amiodarone compared to the min QTce, resulting in increasing the max-min QTce, SD-QTce, and mean Tcp-e.

Table 2 summarized the change of repolarization parameters with amiodarone in all patients. The RR interval was significantly prolonged after amiodarone, whereas QRS duration was not changed. Among 12-lead ECG, although both the

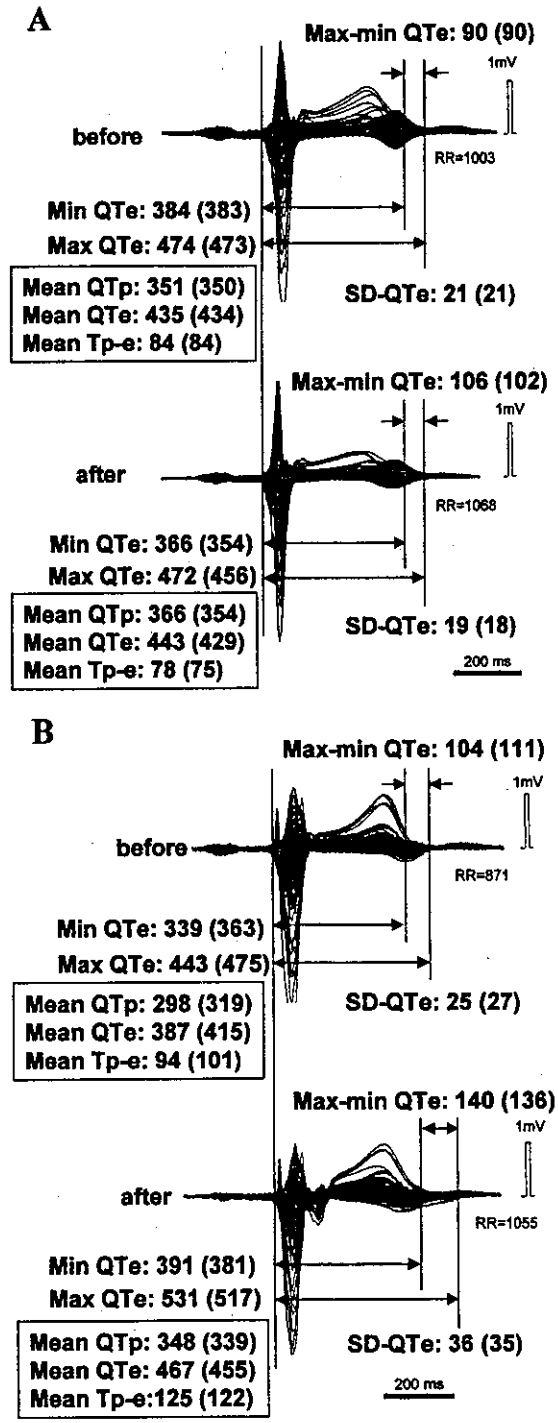

Figure 1. *The superimposed 87-lead ECGs before and after amiodarone in two cases (A and B). All data are presented in ms. Max = maximum value among 87 leads; Min = minimum value among 87 leads; QTe = Q-Tend interval; QTp = Q-Tpeak interval; Tp-e = Tpeak-Tend interval; Max-min QTe = difference between max QTe and min QTe; SD-QTe = standard deviation of QTe among 87 leads; Mean = average value among 87 leads. ( ) = corrected to heart rate by Bazett's method.*

Table II.

Change of Parameters with Chronic Amiodarone

		Before	After	P
	RR	936 ± 137	1017 ± 130	<0.01
	QRS	111 ± 27	120 ± 31	0.14
12-lead	Max QTce	457 ± 41	511 ± 68	<0.01
	Min QTce	394 ± 45	431 ± 49	<0.01
	Max-Min QTce	64 ± 37	80 ± 43	0.053
	SD-QTce	20 ± 13	24 ± 13	0.11
	V5 Tcp-e	90 ± 27	108 ± 45	<0.01
87-lead	Max QTce	470 ± 40	522 ± 60	<0.01
	Min QTce	374 ± 30	400 ± 39	<0.01
	Max-Min QTce	96 ± 30	122 ± 43	<0.01
	SD-QTce	19 ± 7	26 ± 12	<0.01
	Mean QTce	425 ± 37	463 ± 46	<0.01
	Mean QTcp	341 ± 31	363 ± 35	<0.01
	Mean Tcp-e	85 ± 13	101 ± 26	<0.01

All data are presented as the mean ± SD in ms. Max = maximum value among 12 or 87 lead; Min = minimum value among 12 or 87 leads; QTce = corrected Q-Tend interval; Max-Min QTce = maximum minus minimum QTce; SD-QTce = standard deviation of QTce among 12 or 87 leads; QTcp = corrected Q-Tpeak interval; Tcp-e = corrected Tpeak-Tend interval.

max and min QTce were significantly prolonged after amiodarone, the max-min QTce and SD-QTce were not significantly changed (P = 0.053 and P = 0.11, respectively). Among 87-lead ECG, both the max and min QTce were also significantly prolonged after amiodarone; the max QTce was more prolonged compared to the min QTce, thus significantly increasing the max-min QTce and SD-QTce. Moreover, both the mean QTce and mean QTcp were significantly prolonged after amiodarone; the mean QTce was more prolonged compared to the mean QTcp, thus significantly increasing the mean Tcp-e.

Clinical Outcome

Mean follow-up period was 15 ± 10 months after the second recording of body surface ECG during oral amiodarone. The arrhythmic events occurred in 20 of 50 (40%) patients, however no patients had proarrhythmia. Three patients suddenly died, probably due to VT, and the other 17 patients developed recurrence of sustained monomorphic VT. The recurrent VT had the same QRS morphology as those documented before administrating amiodarone in 15 of the 17 patients. We discontinued treating with amiodarone in 11 of the 17 patients as a result of recurrent VT. There was no difference in the amiodarone loading and maintenance doses between patients with (353 ± 78 mg/day and 197 ± 32 mg/day, respectively) and without (374 ± 81 mg/day and 194 ± 34 mg/day, respectively) recurrence of VT/VF. We implanted an implantable cardioverter defibrillator (ICD) in 15 (30%) of the 50 patients, and VT was detected by ICD in 6 (40%) of the 15 patients. In the remaining 35 patients without ICD, 14 (40%) patients had recurrence of VT or died suddenly. Thus, there is no detection bias for the arrhythmic events between patients with and without ICD. Moreover, there was no significant difference in the clinical outcome between patients with prior myocardial infarction, dilated cardiomyopathy, and arrhythmogenic right ventricular cardiomyopathy.

Predictors of Arrhythmic Events

Univariate predictors of arrhythmic events are shown in Table III. Age, gender, basal heart disease, LVEF, NYHA functional class, previous VT rate, and medical treatments were not related to further arrhythmic events. No parameters from the 12-lead ECGs were significantly correlated to further arrhythmic events. However, repolarization parameters from the 87-lead ECG, such as post max QTce, post max-min QTce, post SD-QTce, and post mean Tcp-e, were significantly correlated to further arrhythmic events. The ROC analysis showed that these repolarization parameters from the 87-lead ECG were superior to those from the 12-lead ECG, and the post max-min QTce from 87-lead was the strongest parameter to predict further arrhythmic events (Fig. 2). Moreover, the ROC curves indicated the post max QTce of 510 ms, post max-min QTce of 106 ms, post SD-QTce of 22.4 ms, and post mean Tcp-e of 100 ms as the best cutoff point of each parameters.

For the multivariate Cox analysis, clinical variables (age, gender, basal heart disease, LVEF) and the post max-min QTce from the 87-lead ECG, which was the strongest predictor for arrhythmic events, were entered as independent categorical variables. As a result, post max-min QTce ≥106 ms was a significant predictor of further arrhythmic events after amiodarone treatment (hazard ratio = 10.4, 95%CI: 2.7 to 40.5, P = 0.0008). Kaplan-Meier event-free probability curves showed that patients with post max QTce ≥510 ms had higher arrhythmic events after amiodarone than those < 510 ms (P = 0.0003, Fig. 3A). Similarly, patients with post max-min QTce ≥106 ms, post SD-QTce ≥22.4 ms or post mean Tcp-e ≥100 ms had highly arrhythmic events than those <106 ms, <22.4 ms, or <100 ms (P < 0.0001, P = 0.0007, and P = 0.002, respectively. Fig. 3B, 3C, 3D). The sensitivity, specificity, positive and negative predictive values, and accuracy in these

Table III.

Univariate Analysis of Arrhythmic Events after Chronic Amiodarone

Variables	Parameter Estimate	Hazard Ratio	95% CI	P value
Age	0.015	1.02	0.97–1.06	0.50
Gender (M)	0.010	1.01	0.34–3.02	0.98
Prior MI	0.085	1.09	0.45–2.63	0.85
LVEF < 30%	0.175	1.19	0.49–2.92	0.70
NHYA ≥ 2	0.356	1.43	0.55–3.73	0.47
VT rate	−0.011	0.99	0.97–1.01	0.20
ACE-I	−0.454	0.64	0.25–1.61	0.34
β-blocker	−0.459	0.63	0.23–1.78	0.38
digitalis	0.396	1.49	0.58–3.84	0.41
pre-Max QTce (/ms)	0.005	1.005	0.99–1.02	0.39
post-Max QTce (/ms)	0.007	1.007	1.00–1.01	0.008
pre-Min QTce (/ms)	0.005	1.005	0.99–1.02	0.49
post-Min QTce (/ms)	0.002	1.002	0.99–1.01	0.72
pre-Max-Min QTce (/ms)	0.003	1.003	0.99–1.02	0.63
post-Max-Min QTce (/ms)	0.015	1.015	1.01–1.02	0.0005
pre-SD-QTce (/ms)	0.008	1.008	0.95–1.07	0.79
post-SD-QTce (/ms)	0.04	1.04	1.01–1.07	0.007
pre-Mean QTce (/ms)	0.004	1.004	0.99–1.02	0.52
post-Mean QTce (/ms)	0.007	1.007	0.99–1.02	0.07
pre-Mean QTcp (/ms)	0.003	1.00	0.99–1.02	0.68
post-Mean QTcp (/ms)	0.004	1.00	0.99–1.02	0.56
pre-Mean Tcp-e (/ms)	0.016	1.02	0.98–1.05	0.37
post-Mean Tcp-e (/ms)	0.018	1.018	1.01–1.03	0.004

pre = before amiodarone; post = after amiodarone. Abbreviations as in Table I and Table II.

parameters for further arrhythmic events were shown in Table IV.

Change of Dispersions and VT/VF Recurrence

Figure 4 illustrates a scatter plot of the data about changes of max-min QTce (ΔSDR) and mean Tcp-e (ΔTDR) with amiodarone in patients with and without recurrence of VT/VF. The ΔSDR and ΔTDR were significantly larger in patients with VT/VF recurrence after amiodarone than those with no recurrence of VT/VF (49 ± 34 ms vs 8 ± 33 ms; $P < 0.001$, and 27 ± 34 ms vs 8 ± 15 ms; $P < 0.05$, respectively).

Discussion

Effect of Amiodarone on Spatial and Transmural Dispersion of Repolarization

Amiodarone is one of the most potent antiarrhythmic drugs in preventing life-threatening arrhythmias.[17] Several clinical studies demonstrated that amiodarone prolonged the QT (QTc) interval but did not increase QT (QTc) dispersion,[20–22] contributing to a very low incidence of TdP arrhythmias.[18,19] Experimental studies in dog model by van Opstal et al.[19] and in isolated rabbit heart by Zabel et al.[26] suggested that the low incidence of TdP with amiodarone was due to the homogenous local ventricular repolarization. However, the standard 12-lead ECG had too small number of leads to cover the whole area of body surface, therefore QT (QTc) dispersion from the 12-lead ECG could not always reflect spatial dispersion of local ventricular repolarization from the whole heart. Our results showed that the baseline max-min QTce obtained from the 87-lead ECG was larger than that from the 12-lead ECG. Therefore, the 87-lead body surface ECGs might reflect in more detail the spatial heterogeneity of ventricular repolarization. Moreover, our results showed that the max-min QTce and SD-QTce was increased after amiodarone in patients with VT/VF recurrence but not in patients without VT/VF recurrence, which may represent the arrhythmogeneity of the increase in SDR.

Recent experimental studies under long QT conditions suggested that increasing TDR across the ventricular wall was linked to ventricular

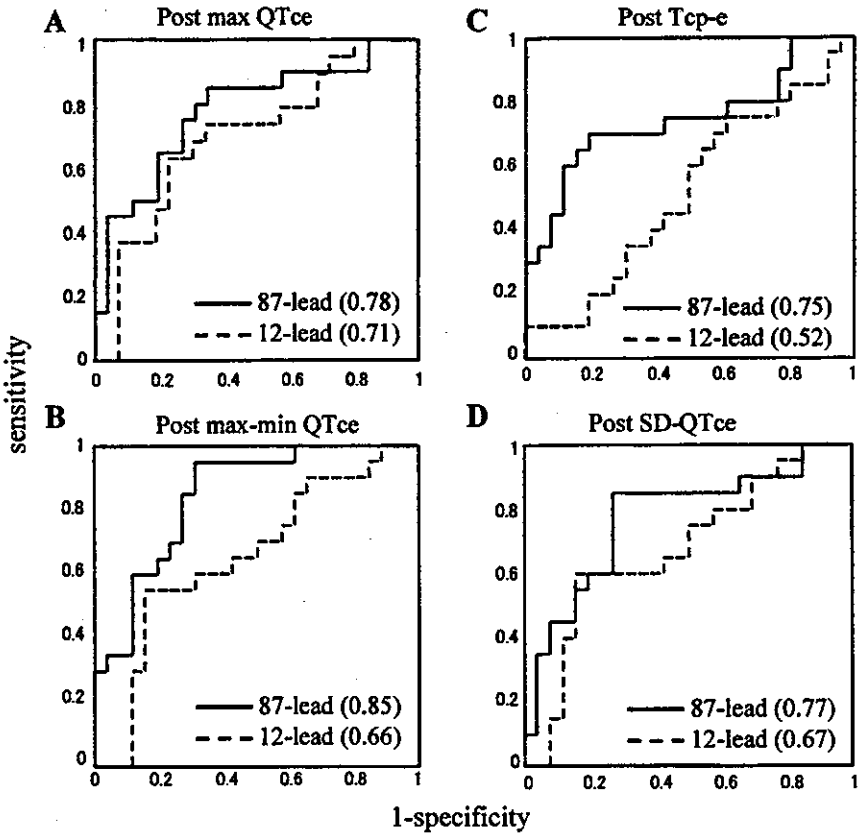

Figure 2. *Receiver operating characteristics curves for the post max QTce, post max-min QTce, post Tcp-e, and post SD-QTce from 87-lead ECG (solid line) and the 12-lead ECG (dotted line) in predicting arrhythmic events after amiodarone. ( ) = area of under curve.*

arrhythmias,[10–12] and that the Tp-e interval in the transmural ECG reflected TDR.[13] Previous experimental studies reported that chronic amiodarone reduced TDR in canine and human hearts.[23,24] These findings suggested that the decrease in TDR with chronic amiodarone, may in part contribute to its antiarrhythmic effect as well as low incidence of proarrhythmias. This study is the first one to demonstrate the change of Tcp-e interval with chronic oral amiodarone, showing that chronic amiodarone slightly but significantly increased the mean Tcp-e, which may relate to the arrhythmogenesis. However, our data also suggested that the mean Tcp-e was not so much increased in patients without VT/VF recurrence after amiodarone compared to those with VT/VF recurrence (Fig. 4). These results are consistent with the report by Merot et al.[25] that chronic amiodarone induced a moderate QT prolongation without affecting TDR.

Prognostic Value of QT Interval, and Spatial and Transmural Dispersions

Amiodarone has differential effects of the two component delayed rectifier K^+ currents: rapidly component (I_{Kr}) and slowly component (I_{Ks}). Kamiya et al. reported that short-term treatment of amiodarone inhibited primarily I_{Kr}, whereas long-term treatment reduced I_{Ks} in the rabbit ventricular myocardium.[16] Lynch et al. suggested that selective blockade of I_{Ks} was useful to prevent ventricular arrhythmias even though the QTc interval was modestly (+7%) increased.[27] Recent studies suggested the excessive prolonged QTc interval was associated with the increase in mortality in patients with dofetilide treatment,[28] and advanced heart failure.[29] These previous studies have supported our data that patients without prolonged max QTce (< 510 ms) after chronic amiodarone had less recurrence of VT/VF compared to those with the excessive prolonged max QTce (≥510 ms).

On the other hand, several studies have investigated the value of QT dispersion in the 12-lead ECG for predicting ventricular arrhythmias or other adverse events in various cardiac diseases,[5,6] but the results are controversial.[30,31] Previous retrospective studies suggested no significant relationship between QT dispersion in the 12-lead ECG and further arrhythmic events after amiodarone.[20,21] Our results also showed no significant correlation between the repolarization parameters from the 12-lead ECG and further arrhythmic events after amiodarone. Although the variability of data in max QTce from the 12-lead ECG were not so different from that of the

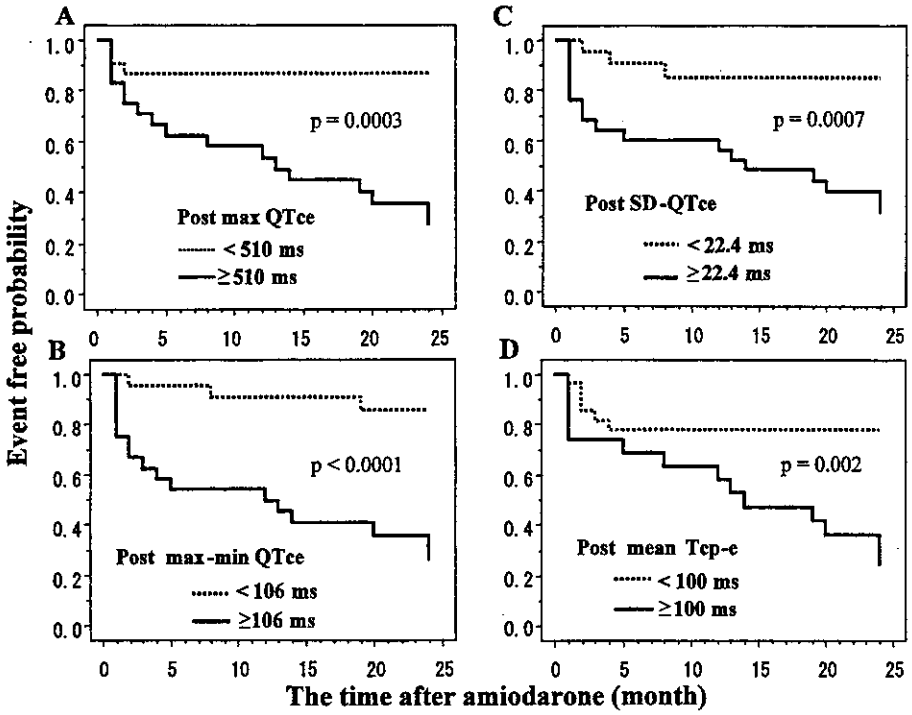

Figure 3. *Kaplan-Meier event-free probability curves (arrhythmic event) for patient groups stratified by above and below median value of maximum QTce after amiodarone (post max QTce) (panel A), max-min QTce after amiodarone (post max-min QTce) (panel B), standard deviation of QTce after amiodarone (post SD-QTce) (panel C), and mean Tcp-e after amiodarone (post mean Tcp-e) (panel D).*

87-lead ECG (Table II), the 87-lead ECG might represent a local ventricular repolarization more accurately compared with 12-lead ECG. Therefore, the excessive prolongation of post max QTce, post max-min QTce, post SD-QTce, and post mean Tcp-e from the 87-lead ECG but not from the 12-lead ECG could predict further arrhythmic events after amiodarone.

Why are the max QT interval and both the spatial and transmural dispersions, excessively increased in some patients but not in other patients? Yuan et al. reported in cat heart that myocytes in noninfarct regions remote from the scar were hypertrophied and reduced in I_{Kr} density.[32] Under condition of the I_{Kr} dysfunction, the repolarization current might more depend on I_{Ks}, therefore blockade of I_{Ks} by chronic amiodarone is expected to markedly prolong APD and QT interval. Several ionic currents notably sodium/calcium exchange, transient outward current, and chloride current together with the I_{Kr} and I_{Ks} have altered in failing heart. Moreover, a recent study reported that the late sodium current (I_{Na}) is a novel target for amiodarone in human failing heart.[33] Thus, the remodeling of some ionic currents in failing heart might cause the excessive prolongation of post max QTce after amiodarone.

Table IV.

Predictors of Arrhythmic Events

	Se	Sp	PPV	NPV	Ac
post-Max QTce ≥ 510 ms	80	69	67	82	74
post-SD-QTce ≥ 22.4 ms	85	73	71	86	78
post-Max-Min QTce ≥ 106 ms	85	73	71	86	78
post-Mean Tcp-e ≥ 100 ms	70	81	74	78	76

post = after amiodarone; Se = sensitivity; Sp = specificity; PPV = positive predictive value; NPV = negative predictive value; Ac = accuracy. Abbreviations as in Table I and Table II.

Study Limitation

First, this study attempted to determine the max-min QTce and SD-QTce as indexes of SDR, and the mean Tcp-e as an index of TDR. While the experimental studies using canine wedge preparation have suggested a correlation between Tpeak-Tend interval in the transmural ECG and

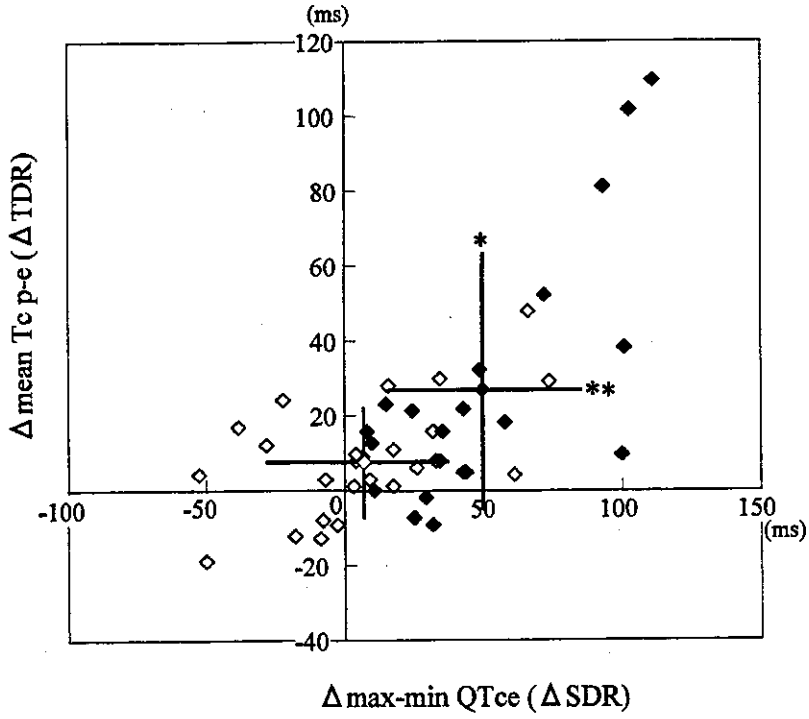

Figure 4. *A scatter plot of chronic amiodarone induced changes of the max-min QTce and mean Tcp-e (Δ SDR and ΔTDR) in patients with VT/VF recurrence (closed square) and without VT/VF recurrence (open square). *P < 0.05; **P < 0.01.*

TDR, there is no evidence that the max QTce in the 87-lead ECG truly reflects the longest repolarization time and the putative SDR and TDR measured from the body surface ECG actually reflect those in the human heart. Second, the long-term reproducibility of the measurement of QT interval, SDR, and TDR could not be assessed. Moreover, in case of the flat or low amplitude T wave (<0.05 mV), Q-Tpeak, Q-Tend, and QTend dispersion, TDR are methodologically unidentifiable, thus we excluded almost 5% of leads with the criteria.

Acknowledgments: We gratefully acknowledge the expert statistical assistance of Nobuo Shirahashi, from Novartis Parma Co., and the technical assistance of Hiroshi Date, Syuji Hashimoto, Sonoe Ito, Itsuko Murakami, Etsuko Ohnishi and Norio Tanaka.

References

1. Kuo CS, Munakata K, Reddy CP, et al. Characteristics and possible mechanism of ventricular arrhythmia dependent on the dispersion of action potential durations. Circulation 1983; 67:1356–1367.
2. Zabel M, Portnoy S, Franz M. Electrocardiographic indexes of dispersion of ventricular repolarization: An isolated heart validation study. J Am Coll Cardiol 1995; 25:746–752.
3. Zabel M, Lichtlen PR, Haverich A, et al. Comparison of ECG variables of dispersion of ventricular repolarization with direct myocardial repolarization measurements in the human heart. J Cardiovasc Electrophysiol 1998; 9:1279–1284.
4. Priori SG, Napolitano C, Diehl L, et al. Dispersion of the QT interval. A marker of therapeutic efficacy in the idiopathic long QT syndrome. Circulation 1994; 89:1681–1689.
5. Perkiömäki JS, Koistinen MJ, Yli-Mäyry S, et al. Dispersion of QT interval in patients with and without susceptibility to ventricular tachyarrhythmias after previous myocardial infarction. J Am Coll Cardiol 1995; 26:174–179.
6. Grancy JM, Garratt CJ, Woods KL, et al. QT dispersion and mortality after myocardial infarction. Lancet 1995; 345:945–948.
7. Shimizu W, Kamakura S, Ohe T, et al. Diagnostic value of recovery tine measured by body surface mapping in patients with congenital long QT syndrome. Am J Cardiol 1994; 74:780–785.
8. Aiba T, Inagaki M, Shimizu W, et al. Recovery time dispersion measured from 87-lead body surface potential mapping as a predictor of sustained ventricular tachycardia in patients with idiopathic dilated cardiomyopathy. J Cardiovasc Electrophysiol 2000; 11:968–974.
9. Shimizu W, Kamakura S, Kurita T, et al. Influence of epinephrine, propranolol, and atrial pacing on spatial distribution of recovery time measured by body surface mapping in congenital long QT syndrome. J Cardiovasc Electrophysiol 1997; 8:1102–1114.
10. Shimizu W, Antzelevitch C. Sodium channel block with mexiletine is effective in reducing dispersion of repolarization and preventing torsade de pointes in LQT2 and LQT3 models of the long QT syndrome. Circulation 1997; 96:2038–2047.
11. Shimizu W, Antzelevitch C. Cellular basis for the electrocardiographic features of LQT1 form of the long QT syndrome. Effects of β adrenergic agonists, antagonists and sodium channel blockers on transmural dispersion of repolarization and torsade de pointes. Circulation 1998; 98:2314–2322.
12. Shimizu W, Antzelevitch C. Cellular and ionic basis for T wave alternans under long QT conditions. Circulation 1999; 99:1499–1507.
13. Yan GX, Antzelevitch C. Cellular basis for the normal T wave and the electrocardiographic manifestations of the long QT syndrome. Circulation 1998; 98:1928–1936.
14. Tanabe Y, Inagaki M, Kurita T, et al. Sympathetic stimulation produces a greater increase in both transmural and spatial dispersion of repolarization in LQT1 than LQT2 forms of congenital long QT syndrome. J Am Coll Cardiol 2001; 37:911–919.
15. Shimizu W, Tanabe Y, Aiba T, et al. Differential effects of β-blockade on dispersion of repolarization in absence and presence of sympathetic stimulation between LQT1 and LQT2 forms of congenital long QT syndrome. J Am Coll Cardiol 2002; 39:1984–1991.

16. Kamiya K, Nishiyama A, Yasui K, et al. Short- and long-term effects of amiodarone on the two components of cardiac delayed rectifier K^+ current. Circulation 2001; 103:1317–1324.
17. Amiodarone Trials Meta-analysis Investigators. Effect of prophylactic amiodarone on mortality after acute myocardial infarction and in congestive heart failure: Meta-analysis of individual data from 6500 patients in randomized trials. Lancet 1997; 350:1417–1424.
18. Hii JTY, Wyse DG, Gillis AM, et al. Precordial QT interval dispersion as a marker of torsade de pointes, disparate effects of class Ia antiarrhythmic drugs and amiodarone. Circulation 1992; 86:1376–1382.
19. van Opstal JM, Schoenmakers M, Verduyn SC, et al. Chronic amiodarone evokes no torsade de pointes arrhythmias despite QT lengthening in an animal model of acquired long-QT syndrome. Circulation 2001; 104:2722–2727.
20. Meierhenrich R, Helguera ME, Kidwell GA, et al. Influence of amiodarone on QT dispersion in patients with life-threatening ventricular arrhythmias and clinical outcome. Int J Cardiol 1997; 60:289–294.
21. Grimm W, Steder U, Menz V, et al. Effect of amiodarone on QT dispersion in the 12-lead standard electrocardiogram and its significance for subsequent arrhythmic events. Clinical Cardiol 1997; 20:107–110.
22. Cui G, Sen L, Sager P, et al. Effects of amiodarone, sematilide, and sotalol on QT dispersion. Am J Cardiol 1994; 74:896–900.
23. Sicouri S, Moro S, Litovsky S, et al. Chronic amiodarone reduced transmural dispersion of repolarization in the canine heart. J Cardiovasc Electrophysiol 1997; 8:1269–1279.
24. Drouin E, Lande G, Charpentier F. Amiodarone reduces transmural heterogeneity of repolarization in the human heart. J Am Coll Cardiol 1998; 32:1063–1067.
25. Merot J, Charpentier F, Poirier JM, et al. Effects of chronic treatment by amiodarone on transmural heterogeneity of canine ventricular repolarization in vivo: Interactions with acute sotalol. Cardiovasc Res 1999; 44:303–314.
26. Zabel M, Hohnloser S, Behrens S, et al. Differential effects of d-sotalol, quinidine, and amiodarone on dispersion of ventricular repolarization in the isolated rabbit heart. J Cardiovasc Electrophysiol 1997; 8:1239–1245.
27. Lynch JJ, Houle MS, Stump GL, et al. Antiarrhythmic efficacy of selective blockade of cardiac slowly activation delayed rectifier current, I_{Ks}, in canine model of malignant ventricular arrhythmia. Circulation 1999; 100:1917–1923.
28. Brendorp B, Elming H, Jun L, et al. QTc interval as a guide to select those patients with congestive heart failure and reduced left ventricular systolic function who will benefit from antiarrhythmic treatment with dofetilide. Circulation 2001; 103:1422–1427.
29. Vrtovec B, Delgado R, Zewail A, et al. Prolonged QTc interval and high B-type natriuretic peptide levels together predict mortality in patients with advanced heart failure. Circulation 2003; 107:1764–1769.
30. Malik M, Batchvarov VN. Measurement, interpretation and clinical potential of QT dispersion. J Am Coll Cardiol 2000; 36:1749–1766.
31. Zabel M, Klingenheben T, Franz MR, et al. Assessment of QT dispersion for prediction of mortality or arrhythmic events after myocardial infarction, results of a prospective, long-term follow-up study. Circulation 1998; 97:2543–2543.
32. Yuan F, Pinto J, Li Q, et al. Characteristics of I_K and its response to quinidine in experimental healed myocardial infarction. J Cardiovasc Electrophysiol 1999; 10:844–854.
33. Maltsev VA, Sabbah HN, Undrovinas AI. Late sodium current is a novel target for amiodarone: Studies in failing human myocardium. J Mol Cell Cardiol 2001; 33:923–932.

J Appl Physiol 97: 984–990, 2004.
First published May 7, 2004; 10.1152/japplphysiol.00162.2004.

Bionic epidural stimulation restores arterial pressure regulation during orthostasis

Yusuke Yanagiya,[1,2] Takayuki Sato,[1,3] Toru Kawada,[1] Masashi Inagaki,[1] Teiji Tatewaki,[1,4] Can Zheng,[1,2] Atsunori Kamiya,[1] Hiroshi Takaki,[1] Masaru Sugimachi,[1] and Kenji Sunagawa[1]

[1]*Department of Cardiovascular Dynamics, National Cardiovascular Center Research Institute, Suita, Osaka 565-8565;*
[2]*Pharmaceuticals and Medical Devices Agency, Chiyoda-ku, Tokyo 100-0013;*
[3]*Department of Cardiovascular Control, Kochi Medical School, Nankoku, Kochi 783-8505;*
and [4]*Japan Association for the Advancement of Medical Equipment, Bunkyo-ku, Tokyo 113-0033, Japan*

Submitted 13 February 2004; accepted in final form 30 April 2004

Yanagiya, Yusuke, Takayuki Sato, Toru Kawada, Masashi Inagaki, Teiji Tatewaki, Can Zheng, Atsunori Kamiya, Hiroshi Takaki, Masaru Sugimachi, and Kenji Sunagawa. Bionic epidural stimulation restores arterial pressure regulation during orthostasis. *J Appl Physiol* 97: 984–990, 2004. First published May 7, 2004; 10.1152/japplphysiol.00162.2004.—A bionic baroreflex system (BBS) is a computer-assisted intelligent feedback system to control arterial pressure (AP) for the treatment of baroreflex failure. To apply this system clinically, an appropriate efferent neural (sympathetic vasomotor) interface has to be explored. We examined whether the spinal cord is a candidate site for such interface. In six anesthetized and baroreflex-deafferentiated cats, a multielectrode catheter was inserted into the epidural space to deliver epidural spinal cord stimulation (ESCS). Stepwise changes in ESCS rate revealed a linear correlation between ESCS rate and AP for ESCS rates of 2 pulses/s and above (r^2, 0.876–0.979; slope, 14.3 ± 5.8 mmHg·pulses^{-1}·s; pressure axis intercept, 35.7 ± 25.9 mmHg). Random changes in ESCS rate with a white noise sequence revealed dynamic transfer function of peripheral effectors. The transfer function resembled a second-order, low-pass filter with a lag time (gain, 16.7 ± 8.3 mmHg·pulses^{-1}·s; natural frequency, 0.022 ± 0.007 Hz; damping coefficient, 2.40 ± 1.07; lag time, 1.06 ± 0.41 s). On the basis of the transfer function, we designed an artificial vasomotor center to attenuate hypotension. We evaluated the performance of the BBS against hypotension induced by 60° head-up tilt. In the cats with baroreflex failure, head-up tilt dropped AP by 37 ± 5 mmHg in 5 s and 59 ± 11 mmHg in 30 s. BBS with optimized feedback parameters attenuated hypotension to 21 ± 2 mmHg in 5 s ($P < 0.05$) and 8 ± 4 mmHg in 30 s ($P < 0.05$). These results indicate that ESCS-mediated BBS prevents orthostatic hypotension. Because epidural stimulation is a clinically feasible procedure, this BBS can be applied clinically to combat hypotension associated with various pathophysiologies.

baroreceptors; blood pressure; autonomic nervous system; Shy-Drager syndrome; orthostatic hypotension

THE ARTERIAL BAROREFLEX SYSTEM configures a negative feedback system and reduces arterial pressure (AP) disturbances from external influences (9, 15, 22, 23). Sudden onset of hypotension by orthostatic change occurs as a result of baroreflex failure, despite normal functioning of the cardiovascular system and efferent sympathetic nervous system. This condition is seen in multiple-system atrophy (Shy-Drager syndrome) (21, 22, 30) as well as spinal cord injuries (7, 17). Current treatments, such as salt loading (19, 33), cardiac pacing (1, 14), and pharmacological interventions (2, 3, 12, 20), fail to prevent the orthostatic hypotension. These therapies often result in an unwanted increase in AP in the supine position and neither restore nor reproduce the function of the feedback system that forms the basis of AP control (See DISCUSSION).

Previously, our laboratory developed a bionic baroreflex system (BBS) that substitutes the defective vasomotor center with an artificial controller (i.e., an artificial vasomotor center) to restore the native baroreflex function (24, 26). In these animal studies, the celiac ganglion was exposed by laparotomy and stimulated directly as the efferent neural interface in the BBS. However, for clinical application of the BBS, a less invasive and more stable electrical stimulation method is required.

In the present study, we examined the hypothesis that the spinal cord is a candidate site for the efferent neural interface in our bionic strategy. Epidural spinal cord stimulation (ESCS) has been used for the management of patients with malignant neoplasm, angina pectoris, and peripheral ischemia (6, 29). Stimulating the dorsal part of the spinal cord changes sympathetic nerve activity, AP in animals (11, 32) and heart rate in humans (18). If we can delineate how ESCS affects AP quantitatively, then this may lead to clinical application of the BBS. We studied the feasibility of ESCS-mediated BBS using an animal model of central baroreflex failure.

MATERIALS AND METHODS

Study design. BBS is a negative feedback system and consists of two components: peripheral effectors and the artificial vasomotor center (Fig. 1). Peripheral effectors change AP in response to ESCS. The artificial vasomotor center (controller) determines the ESCS rate in response to changes in AP. Using BBS, we computer programmed the artificial vasomotor center and substituted the defective vasomotor center with an artificial vasomotor center.

For this purpose, we first characterized the static as well as dynamic responses of the peripheral effectors. With this knowledge, we then designed an artificial vasomotor center using simulation to delineate the parameters for obtaining optimal AP response. Finally, we evaluated the performance of the ESCS-mediated BBS in cats during orthostatic AP changes.

Animals and surgical procedures. Animals were cared for in strict accordance with the "Guiding Principles for the Care and Use of Animals in the Field of Physiological Sciences," approved by the Physiological Society of Japan. Six adult cats of either sex, weighing

Address for reprint requests and other correspondence: M. Sugimachi, Dept. of Cardiovascular Dynamics, National Cardiovascular Center Research Institute, 5-7-1 Fujishirodai, Suita 565–8565, Japan.

The costs of publication of this article were defrayed in part by the payment of page charges. The article must therefore be hereby marked "*advertisement*" in accordance with 18 U.S.C. Section 1734 solely to indicate this fact.

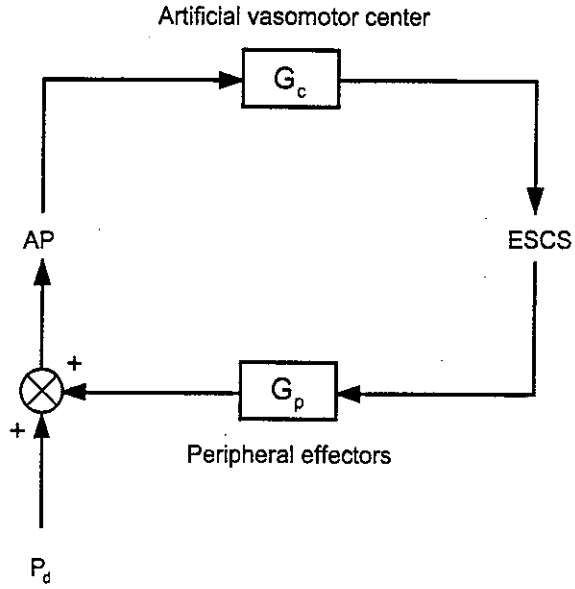

Fig. 1. Simplified diagram of bionic baroreflex system (BBS) using epidural spinal cord stimulation (ESCS). Peripheral effectors change arterial pressure (AP) in response to ESCS. The artificial vasomotor center determines ESCS rate in response to changes in AP. Transfer function of the peripheral effectors (G_p) cannot be controlled, but the vasomotor center transfer function (G_c) can be computer programmed as needed. P_d, pressure disturbance to AP.

1.6–3.7 kg, were premedicated with ketamine (5 mg/kg im) and then anesthetized by intraperitoneal injection (1.0 ml/kg) of a mixture of urethane (250 mg/ml) and α-chloralose (40 mg/ml).

For AP measurement, a high-fidelity pressure transducer (SPC-320, Millar Instruments, Houston, TX) was placed in the aortic arch via the right femoral artery. Pancronium bromide (0.3 mg/kg) was administered to prevent muscular activity. The cats were mechanically ventilated with oxygen-enriched room air. Body temperature was maintained at around 38°C with a heating pad. To produce the baroreflex failure model, the carotid sinus, aortic depressor, and vagal nerves were sectioned bilaterally. The rationale for using baroreceptor-deafferentiated animals as the baroreflex failure model is that, in patients with multiple-system atrophy, the reason for sudden hypotension induced by orthostatic change is a lack of reflex control of AP sensed at the baroreceptors.

A partial laminectomy was performed in the L_3 vertebra to expose the dura mater. A multielectrode catheter with interelectrode distance of 10 mm was introduced rostrally ~7 cm into the epidural space. The stimulating electrodes were positioned on the dorsal surface of the spinal cord within T_{12}, T_{13}, and L_1. These spinal levels were selected because our preliminary studies showed that ESCS to these levels produced greater AP response compared with other spinal levels. The catheter was connected to an isolated electric stimulator (SS-102J and SEN7203, Nihon Kohden, Tokyo, Japan) via a custom-made, constant-voltage amplifier. The stimulator was controlled with a laboratory computer (PC9801FA, NEC, Tokyo, Japan).

Data recording for characterizing AP response to ESCS. To characterize the static as well as dynamic AP responses to ESCS, we measured AP responses while changing ESCS rate. To estimate static response, we changed the ESCS rate sequentially in stepwise increments and decrements. Each stimulation step was maintained for 90 s. To estimate dynamic response, we randomly changed the ESCS rate, according to a binary white noise sequence with a minimum sequence length of 1 s. In both protocols, the stimulation voltage was fixed at 5 V, and the pulse width of the stimulus was 1 ms. While the stimulation was given, ESCS rate and AP were digitized at a rate of 200 Hz with a 12-bit resolution analog-to-digital converter [AD12–8 (PM), Contec, Osaka, Japan] and stored in another laboratory computer (PC98-NX VA70J, NEC). In this study, "ESCS rate" is defined as the number of stimulation pulses per second and is distinguished from the term "frequency," which refers to how frequently ESCS rate changes.

Estimation of static AP response parameters. We parameterized the static AP response to ESCS. Each steady-state AP value was obtained by averaging the AP during the last 10 s of each ESCS step. Stimulation at low-ESCS rate decreased AP, but stimulation at higher rates increased AP. We fit both responses together to a linear regression model of AP vs. ESCS rate. We determined the rate at which the pressor and depressor effects balanced and designated it the offset stimulation rate (s_o).

Estimation of peripheral effector transfer function. The transfer function of the peripheral effector was estimated by using a white noise method described in detail elsewhere (10, 13, 16, 24–26, 31). Briefly, on the basis of the resampled data at 10 Hz, the linear transfer function from ESCS rate to AP was calculated as a quotient of the ensemble average of cross-power between the two and that of ESCS rate power. The transfer function was calculated up to 0.5 Hz with a resolution of 0.0098 Hz. We parameterized the transfer function by using an iterative, nonlinear, least squares fitting technique (10).

Design of central characteristics and implementation by the artificial vasomotor center. Based on the parameterized effector transfer function, we designed the vasomotor center transfer function using computer simulation. The characteristics of the vasomotor center have been identified as derivative characteristics in rabbits and rats (10, 13, 25). We did not have the corresponding data for cats but assumed that they resembled those in rabbits and rats. We adjusted the parameters by simulation, aiming to attenuate hypotension to ~20 mmHg within 5 s and to ≤10 mmHg at 30 s. We implemented designed transfer function by the artificial vasomotor center with convolution algorithm (see APPENDIX).

Head-up tilt tests. The efficacy of the BBS against orthostatic stress was evaluated in each animal by the head-up tilt (HUT) test. We placed baroreflex failure animals in a prone position on a custom-made tilt table and measured AP responses to 60° HUT, with or without BBS activation. In the absence of BBS control, we fixed the ESCS rate at s_o, irrespective of AP changes. The BBS was activated by sending ESCS command to the stimulator, as calculated by the artificial vasomotor center in response to AP change. Tilt angle, ESCS rate, and AP were stored in a laboratory computer.

Statistical analysis. All data are presented as means ± SD. We analyzed AP responses at 5 and 30 s after HUT. AP changes from control value were compared among protocols by using repeated-measures analysis of variance followed by Dunnett's multiple-comparison procedure (8). Differences were considered significant when $P < 0.05$.

RESULTS

Figure 2*A* is a representative example of static AP response to stepwise ESCS changes. Stepwise increases of ESCS rate produced a depressor response initially at low-ESCS rate and a pressor response at higher rates, and subsequent decreases of ESCS rate produced almost perfect reversal of AP changes. The relationship between AP and ESCS rate appeared nonlinear as a whole (Fig. 2*B*, *top*). However, for ESCS rates of 2 pulses/s and above, there is a linear relationship (r^2 = 0.964, AP = 16.0 × ESCS + 44.0, s_o = 3.2 pulses/s; Fig. 2*B*). A linear relationship during ESCS was found in all animals [r^2, 0.876–0.979 (median, 0.959) slope, 14.3 ± 5.8 mmHg·pulses^{-1}·s; pressure axis intercept, 35.7 ± 25.6 mmHg; s_o, 4.9 ± 2.5 pulses/s]. The following protocols were performed by using this linear ESCS range.

Figure 3*A* is a representative example of dynamic AP response to ESCS. We selected low- and high-stimulation rates that produced depressor and pressor responses, respectively,

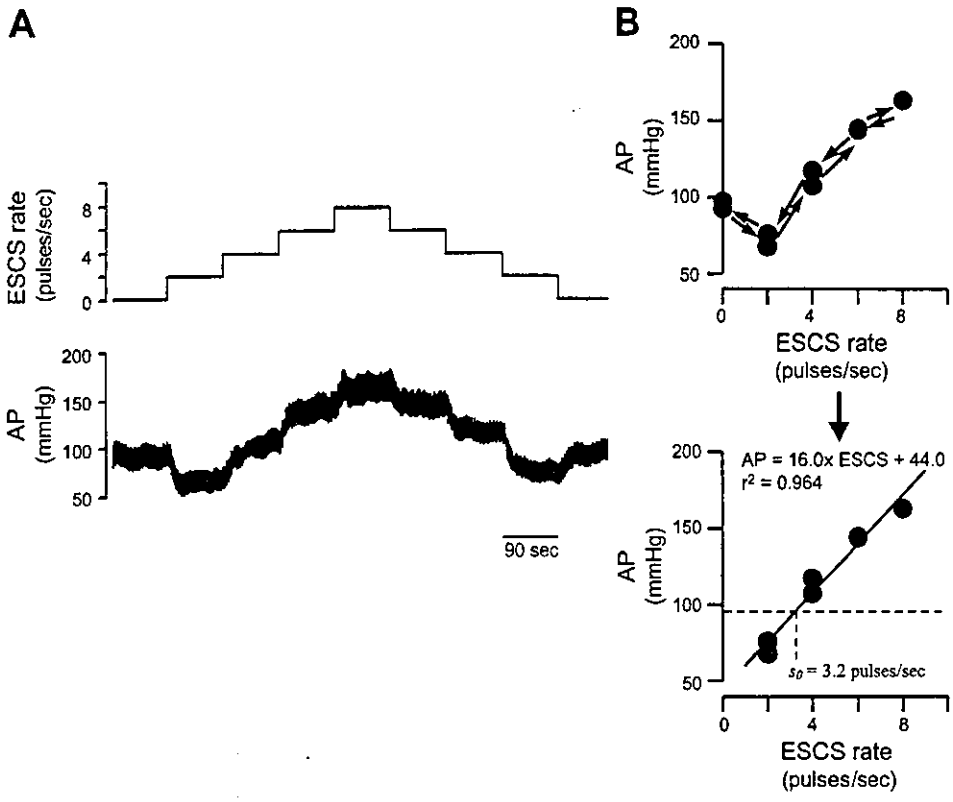

Fig. 2. *A*: representative time series of static AP response to ESCS. Stepwise increases of ESCS rate produced a depressor response initially at low-ESCS rate and a pressor response at higher rates, and subsequent decreases of ESCS rate produced almost perfect reversal of AP changes. *B*: procedures to estimate steady-state relationship between AP and ESCS rate. Each steady-state AP value was plotted against ESCS rate (*top*). Although the relationship between AP and ESCS rate appears nonlinear as a whole, linear regression analysis was conducted for the data obtained during ESCS (2, 4, 6, and 8 Hz), omitting the values before and after ESCS (0 Hz). A linear relationship is obtained. The value s_o represents the stimulation rate where pressor and depressor responses balance.

and stimulated the spinal cord, according to a binary white noise sequence. AP did not respond to fast changes in ESCS rate, but appeared to respond to slower changes, increasing with high-rate stimulation and decreasing with low-rate stimulation. The estimated transfer function indicated low-pass filter characteristics. Figure 3*B* shows the averaged transfer function from ESCS rate to AP in six animals. The gain decreased as the frequency increased and was attenuated to one-tenth of the lowest frequency at 0.1 Hz. The phase approached zero radian at the lowest frequency, reflecting in-phase changes of ESCS rate and AP. The parameters obtained by the least squares fitting to the second-order, low-pass filter model are as follows: dynamic gain = 16.7 ± 8.3 mmHg·pulses^{-1}·s, natural frequency = 0.022 ± 0.007 Hz, damping coefficient = 2.40 ± 1.07, and lag time = 1.06 ± 0.41 s. The dynamic gain was much higher than the gain at the lowest frequency in the transfer function (Fig. 3*A*) but comparable to the slope obtained in the static protocol. The coherence function was close to unity between 0.01 and 0.4 Hz, indicating that the input-output relation was governed by almost linear

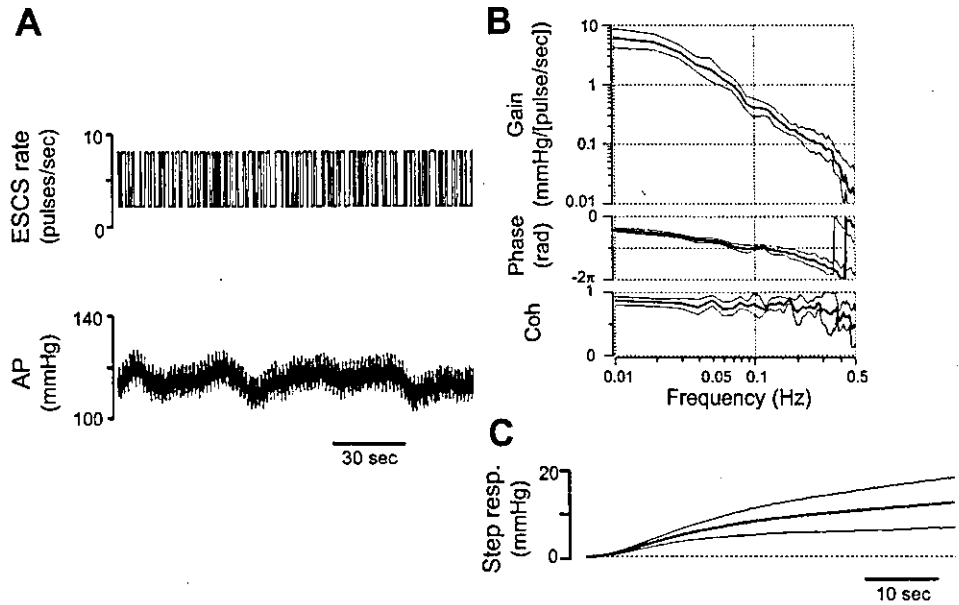

Fig. 3. *A*: representative example of dynamic AP response to ESCS. *B*: averaged transfer functions from ESCS rate to AP, i.e., G_p (gain and phase) and coherence function (Coh). *C*: estimated step response (resp) computed from the transfer function. Data are expressed as means ± SD for 6 cats.

dynamics in this range. To facilitate better understanding of the dynamic AP response to ESCS, the step functions were calculated by time integral of the inverse Fourier transform of the transfer functions. The estimated step functions are averaged and shown in Fig. 3*C*. An initial time lag and overdamped slow AP response to unit step ESCS are evident. The time courses of the estimated step functions were almost identical to but smoother than those of the actually observed AP responses to stepwise ESCS changes, indicating the ability to cancel out noises by the white noise method.

Figure 4 is a representative example of how we designed the vasomotor center transfer function. The steady-state gain is determined simply to match a total baroreflex loop gain of 5. This setting ensures that the steady-state AP fall will be attenuated to 10 mmHg in the case of a depressor stimulus of 60 mmHg. By changing the derivative corner frequency (f_c), we simulated various transient AP responses to orthostatic depressor stimulation. Lower f_c causes unstable oscillation in AP (Fig. 4*B*, *left*), and higher f_c slows AP restoration (Fig. 4*B*, *right*). On the basis of these simulations, f_c = 0.02 Hz was selected in this example (Fig. 4*B*, *middle*, 0.018 ± 0.008 Hz in 6 cats).

Figure 5 shows a representative example of real-time application of BBS to a cat. In the control cat with baroreflex failure, abrupt HUT produced a rapid and then progressive fall in AP by 44 mmHg in 30 s (Fig. 5, *left*). Activation of the simulation-based BBS attenuated the AP fall (Fig. 5, *middle*; AP fall, 25 mmHg in 5 s and 19 mmHg in 30 s) but did not attain the predetermined target (gaps indicated by vertical bars in Fig. 5, *middle* and *right*). If the total loop gain of 5 were preserved, the AP fall should theoretically be attenuated to 44/(1 + 5), or ~7 mmHg, according to the linear control theory. The observed attenuation of 19/44 (=1/2.3) indicated that the actual gain was 1.3 (1 + 1.3 = 2.3). To achieve a total loop gain of 5, we increased the gain of the vasomotor center transfer function by 3.8-fold and reassessed the efficacy of BBS. As a result, AP returned to the predetermined target (Fig. 5, *right*; AP fall, 19 mmHg in 5 s, 7 mmHg in 30 s).

Figure 6 summarizes the results obtained from six cats, demonstrating the effectiveness of the BBS performance. In the cat model of baroreflex failure, HUT decreased AP by 37 ± 5 mmHg in 5 s and by 59 ± 11 mmHg in 30 s. In animals with simulation-based vasomotor center, the initial attenuation (AP fall: 32 ± 7 mmHg in 5 s) was not significant, and the steady-state attenuation (17 ± 8 mmHg in 30 s) did not satisfy the predetermined target. On the other hand, in animals with gain-adjusted vasomotor center (2.4 ± 1.1-fold increase), the BBS achieved both initial and the steady-state targets (21 ± 2 mmHg in 5 s, $P < 0.05$; 8 ± 4 mmHg in 30 s, $P < 0.05$).

DISCUSSION

The present results indicate that AP can be controlled by ESCS and that ESCS-mediated BBS prevents orthostatic hypotension in anesthetized cats. Although the BBS based on simulation alone did not work as predicted during HUT, gain adjustments of the vasomotor center achieved quick and stable restoration of AP.

Necessity of BBS for treatment of central baroreflex failure. Conventional treatments for central baroreflex failure aim at increasing AP. Although they alleviate the hypotension to the extent of preventing syncope, they have adverse effects of causing supine hypertension and enhancing the risk of hypertensive organ disease. Recently, Shannon et al. (28) suggested well-timed water consumption as a treatment for orthostatic hypotension in patients with autonomic failure. Their strategy is superior to conventional treatments because it prevents AP fall if predicted in advance. However, at least a few minutes are necessary for their method to increase AP. This time lag makes it impossible to control AP against sudden or unpredictable AP

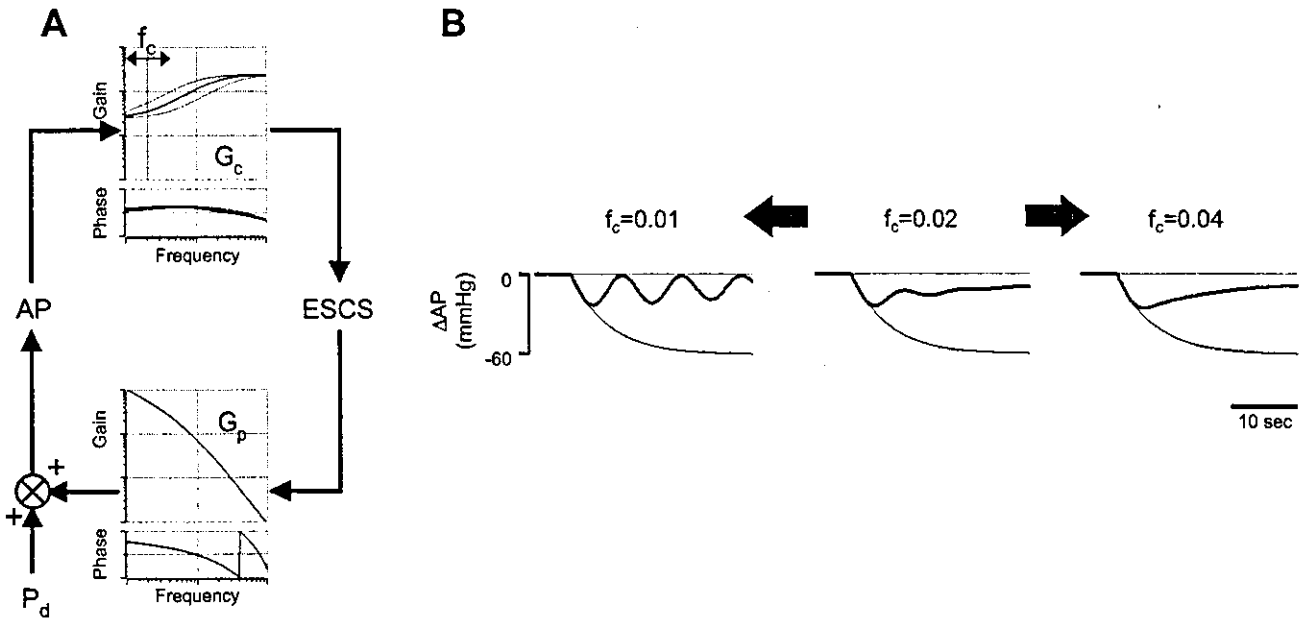

Fig. 4. Representative example of designing the G_c. *A*: schematic diagram of the method of designing the G_c. AP changes in the presence of P_d were simulated by changing the corner frequency (f_c) for derivative characteristic in the G_c. *B*: simulation results of this example. A vasomotor center with f_c of 0.02 Hz restores AP with sufficient speed and stability (center).

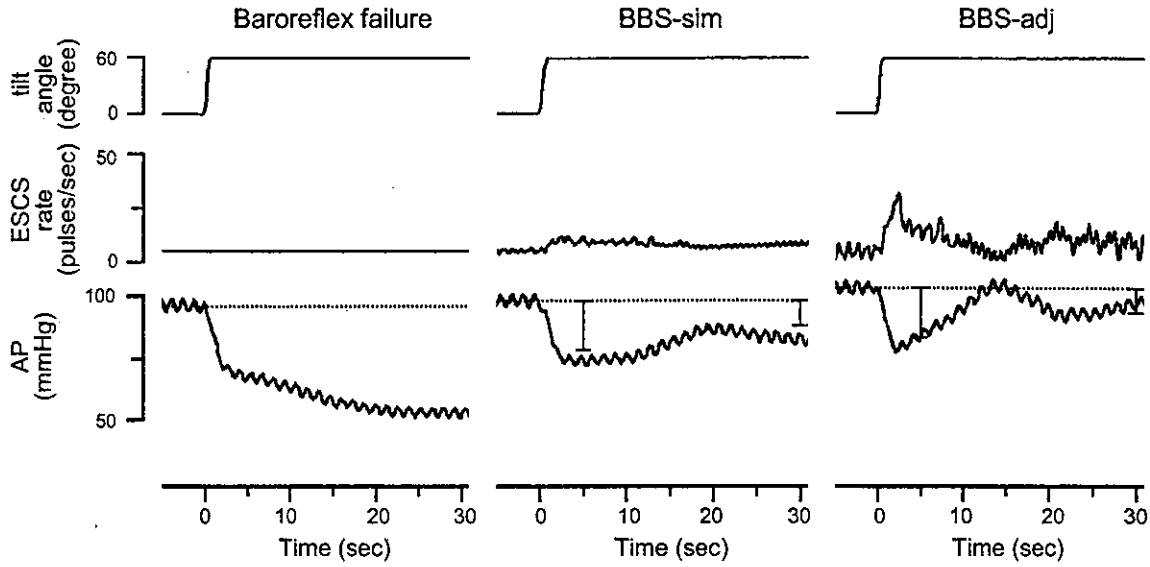

Fig. 5. Representative example of real-time application of the BBS during head-up tilt (HUT). *Left*: in the cat with baroreflex failure, ESCS rate was fixed at 5.0 pulse/s. HUT produced a rapid and then progressive fall in AP. *Middle*: simulation-based BBS (BBS-sim) attenuated the AP fall but did not attain the predetermined target. *Right*: gain adjustment of the vasomotor center (BBS-adj) resulted in quick and sufficient attenuation of AP fall (see text for detail). Vertical bars indicate the ranges of predetermined targets.

fall. None of the treatments attempted so far can prevent sudden orthostatic hypotension because the dynamics of the baroreflex remain impaired.

In contrast, the BBS continuously monitors and controls AP to achieve quick restoration of AP. Because AP is increased via sympathetic pathways, the AP response to the BBS vasomotor center command is as fast as that to the native vasomotor center control. Therefore, the quick, adequate, and stable nature of the native baroreflex system can be restored by the BBS with appropriate settings of the artificial vasomotor center.

Designing the vasomotor center transfer function and parameter adjustments. In a negative feedback system, closed-loop responses to external perturbation are dependent on the dynamic characteristics of the total open-loop transfer function. We assumed that the derivative characteristics in cats are identical to those in rabbits or rats, which have been delineated previously (10, 13, 25). We optimized gain and derivative parameters for each cat so that both speed and stability were achieved.

In animal experiments, however, the simulation results were not fully reproduced. Gain adjustments of the vasomotor center were necessary to attain quick and sufficient attenuation of the AP fall. This discrepancy cannot be explained without considering a possible slope decrease or nonlinearity in peripheral effector characteristics (AP-ESCS relationship) caused by the HUT, or both. Pooling of blood volume in the splanchnic and hindlimb circulation would be a cause for such attenuated AP response. If AP responses during posture change can be de-

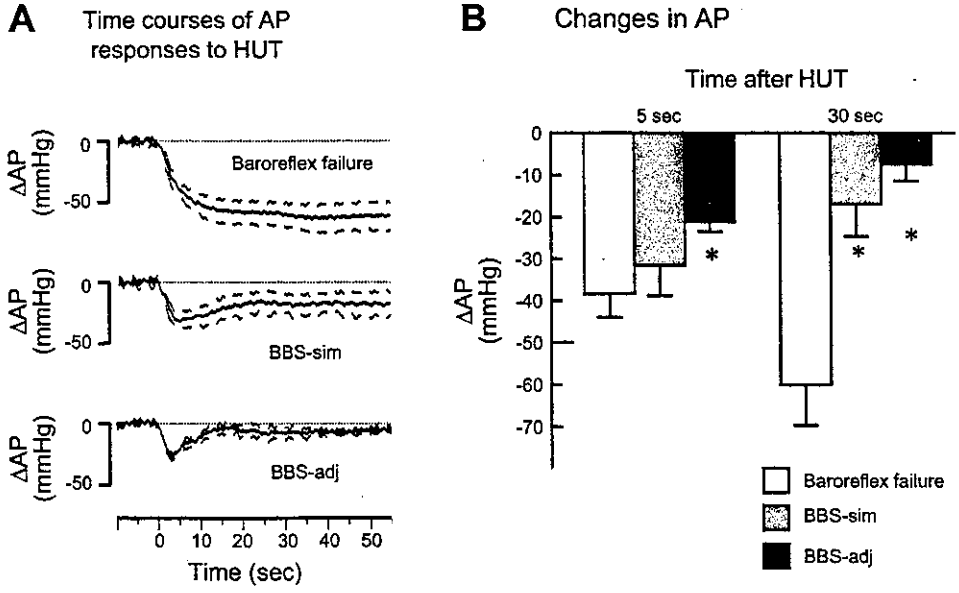

Fig. 6. Summarized results of HUT obtained from 6 cats. *A*: averaged time courses of AP responses to HUT in cats with baroreflex failure (*top*) and with BBS (*middle* and *bottom*). Using the parameters determined from simulation, we found that the BBS (BBS-sim) did not adequately attenuate hypotension in all cats (*middle*). Appropriate gain increase (BBS-adj) was necessary for quick and sufficient attenuation of hypotension (*bottom*). *B*: changes in AP produced by HUT. Data are expressed as means ± SD. *$P < 0.05$ compared with baroreflex failure.

fined quantitatively, then a more elaborate artificial vasomotor center can be developed that automatically adjusts the parameters. Automated adjustments may also be accomplished with adaptive control systems that execute real-time system identification and self-tuning of controller. The present study suggests the necessity of such manipulation of the vasomotor center settings.

Pressor and depressor responses by ESCS. We demonstrated both depressor and pressor responses in AP to ESCS with a linear range (Fig. 2). Earlier studies have shown that dorsal column stimulation produces pressor and depressor responses. Depressor response is produced by a group of dorsal column fibers that project to the dorsal nuclei at the level of C_8 to L_1 and transmit to the fibers that ascend through the dorsal spinocerebeller tracts (4, 27, 32). Pressor response is produced by another group of fibers that ascends or descends through the terminal zone and enter the gray matter. Some of these fibers project to the intermedial lateral columns to activate sympathetic presynaptic fibers. AP responses to ESCS observed in the present study are the results of compound responses in these multiple pathways. Nevertheless, controllability of AP by the BBS is ascertained by a clear linearity between ESCS and AP response in both static and dynamic relationships.

Although we have not confirmed it in the closed-loop condition, depressor response shown in the open-loop condition indicates that ESCS-mediated BBS can attenuate hypertension as well as hypotension. Because an offset ESCS rate (s_o) is applied in the absence of pressure disturbance, lowering ESCS rate would attenuate hypertension to some extent. AP in conscious animals fluctuates between hypertension and hypotension, even in a quiet position (5). The speed of AP restoration is considered sufficient to control these fluctuations.

Future step for clinical application. Clearly, the next step toward clinical application is to demonstrate the safety and the effectiveness of the ESCS-mediated BBS during orthostasis in conscious patients and animals. To study BBS in conscious animals, we have been developing an implantable hardware that enables BBS. Elaboration of such devices is mandatory for its future clinical application by searching the optimal stimulating site and condition that do not cause uncomfortable sensation and muscle twitch. A control algorithm must be developed that overcomes the problem revealed in the present study. The developing implant would be as small and low power as a pacemaker, with the aid of recent LSI technologies, and would be telemetrically programmable. In parallel, we began collaboration with a clinical group to develop ESCS-mediated BBS to suppress sudden hypotension in anesthetized humans during surgery. This study would prove the feasibility of human BBS.

Finally, new methods for long-term manometry are definitely required. Intravascular manometry can be achieved only with long-lasting antithrombotic material. Other indirect methods should be used until we are confident in antithrombotic ability.

Conclusions. As a step toward clinical application of BBS, we demonstrated that AP could be controlled with ESCS. We designed the artificial vasomotor center based on the dynamic characteristics of AP response to ESCS. Although there was a dissociation between the predicted and actual attenuation of AP fall, ESCS-mediated BBS with appropriate gain adjustment was capable of preventing HUT-induced hypotension rapidly, sufficiently, and stably.

APPENDIX

Simulation of AP Restoration and Implementation by the Artificial Vasomotor Center

We modeled the vasomotor center transfer function (G_c) as

$$G_c(f) = K_c \frac{1 + \frac{f}{f_{c1}}j}{\left(1 + \frac{f}{f_{c2}}j\right)\left(1 + \frac{f}{f_{c3}}j\right)} \exp(-2\pi f j L_c) \qquad (A1)$$

where f is frequency, K_c is the steady-state gain of the artificial vasomotor center, f_{c1} is f_c for derivative characteristics, f_{c2} and f_{c3} are corner frequencies for high-cut characteristics, j is an imaginary unit, and L_c is a pure delay. The value f_{c2} was set to $10 \times f_{c1}$, and f_{c3} was set to 1 Hz. These settings attenuate AP pulsation and preserve total baroreflex gain (13). L_c was introduced to simulate the possible time delay of 0.1 s in transforming AP to ESCS rate but was excluded in real-time application to improve AP stability.

The simulation was performed as follows. The block diagram in Fig. 4*A* is represented as

$$AP = G_p \cdot ESCS + P_d$$

$$ESCS = G_c \cdot AP$$

where G_p is transfer function of the peripheral effectors, and P_d is pressure disturbance to AP. Rearranging these formula yields

$$AP = G_c \cdot G_p \cdot AP + P_d \qquad (A2)$$

The time domain representation of *Eq. A2* is

$$\Delta AP(t) = \int g(\tau) \cdot \Delta AP(t - \tau)d\tau + P_d(t) \qquad (A3)$$

where $\Delta AP(t)$ is AP change from control value, and $g(\tau)$ is the impulse response function of the total open-loop transfer function ($G_c \cdot G_p$). To simulate orthostatic hypotension, $P_d(t)$ is set as an exponential AP fall to -60 mmHg with a time constant of 5 s rather than a stepwise fall (see Fig. 6*A*, *top*). We simulated the transient AP response to depressor stimulus while changing f_{c1} in the presence of the negative feedback system.

To implement the designed vasomotor center transfer function, we programmed the artificial vasomotor center to calculate ESCS rate in response to AP changes, according to the following equation:

$$ESCS(t) = \int h(\tau) \cdot \Delta AP(t - \tau)d\tau + s_o$$

where $h(\tau)$ is the impulse response function of the designed vasomotor center transfer function, $\Delta AP(t)$ is AP change from the control value, and s_o is the offset ESCS rate obtained from the static parameterization.

GRANTS

This study was supported by a Grant-in-Aid for Scientific Research (A15200040) from the Japan Society for the Promotion of Science, the Program for Promotion of Fundamental Studies in Health Science of Pharmaceuticals and Medical Devices Agency of Japan, and a Health and Labour Sciences Research Grant (Research on Advanced Medical Technology, H14-nano-002) from the Ministry of Health, Labour and Welfare of Japan.

REFERENCES

1. **Bannister R, da Costa DF, Hendry WG, Jacobs J, and Mathias CJ.** Atrial demand pacing to protect against vagal overactivity in sympathetic autonomic neuropathy. *Brain* 109: 345–356, 1986.

2. **Biaggioni I, Robertson RM, and Robertson D.** Manipulation of norepinephrine metabolism with yohimbine in the treatment of autonomic failure. *J Clin Pharmacol* 34: 418–423, 1994.
3. **Chobanian AV, Volicer L, Tifft CP, Gavras H, Liang CS, and Faxon D.** Mineralocorticoid-induced hypertension in patients with orthostatic hypotension. *N Engl J Med* 301: 68–73, 1994.
4. **Chung JM and Wurster RD.** Ascending pressor and depressor pathways in the cat spinal cord. *Am J Physiol* 231: 786–792, 1976.
5. **Cowley AW Jr, Liard JF, and Guyton AC.** Role of baroreceptor reflex in daily control of arterial blood pressure and other variables in dogs. *Circ Res* 32: 564–576, 1973.
6. **Di Pede F, Lanza GA, Zuin G, Alfieri O, Rapati M, Romano M, Circo A, Cardano P, Bellocci F, Santini M, and Maseri A; Investigators of the Prospective Italian Registry of SCS for Angina Pectoris.** Immediate and long-term clinical outcome after spinal cord stimulation for refractory stable angina pectoris. *Am J Cardiol* 91: 951–955, 2003.
7. **Frankel HL and Mathias CJ.** Severe hypertension in patients with high spinal cord lesions undergoing electro-ejaculation–management with prostaglandin E2. *Paraplegia* 18: 293–299, 1980.
8. **Glantz SA.** *Primer of Biostatistics* (4th ed.). New York: McGraw-Hill, 1997.
9. **Guyton AC, Coleman TG, and Granger HJ.** Circulation: overall regulation. *Annu Rev Physiol* 34: 13–46, 1972.
10. **Ikeda Y, Kawada T, Sugimachi M, Kawaguchi O, Shishido T, Sato T, Miyano H, Matsuura W, Alexander J Jr, and Sunagawa K.** Neural arc of baroreflex optimizes dynamic pressure regulation in achieving both stability and quickness. *Am J Physiol Heart Circ Physiol* 271: H882–H890, 1996.
11. **Illert M and Gabriel M.** Descending pathways in the cervical cord of cats affecting blood pressure and sympathetic activity. *Pflügers Arch* 335: 109–124, 1972.
12. **Kachi T, Iwase S, Mano T, Saito M, Kunimoto M, and Sobue I.** Effect of L-threo-3,4-dihydroxyphenylserine on muscle sympathetic nerve activities in Shy-Drager syndrome. *Neurology* 38: 1091–1094, 1988.
13. **Kawada T, Zheng C, Yanagiya Y, Uemura K, Miyamoto T, Inagaki M, Shishido T, Sugimachi M, and Sunagawa K.** High-cut characteristics of the baroreflex neural arc preserve baroreflex gain against pulsatile pressure. *Am J Physiol Heart Circ Physiol* 282: H1149–H1156, 2002.
14. **Kristinsson A.** Programmed atrial pacing for orthostatic hypotension. *Acta Med Scand* 214: 79–83, 1983.
15. **Malliani A, Pagani M, Lombardi F, and Cerutti S.** Cardiovascular neural regulation explored in the frequency domain. *Circulation* 84: 482–492, 1991.
16. **Marmarelis PZ and Marmarelis VZ.** *Analysis of Physiological Systems: The White-Noise Approach.* New York: Plenum, 1978.
17. **Matthews JM, Wheeler GD, Burnham RS, Malone LA, and Steadward RD.** The effects of surface anaesthesia on the autonomic dysreflexia response during functional electrical stimulation. *Spinal Cord* 35: 647–651, 1997.
18. **Meglio M, Cioni B, Rossi GF, Sandric S, and Santarelli P.** Spinal cord stimulation affects the central mechanisms of regulation of heart rate. *Appl Neurophysiol* 49: 139–146, 1986.
19. **Mehlsen J and Boesen F.** Substantial effect of acute hydration on blood pressure in patients with autonomic failure. *Clin Physiol* 7: 243–246, 1987.
20. **Obara A, Yamashita H, Onodera S, Yahara O, Honda H, and Hasebe N.** Effect of xamoterol in Shy-Drager syndrome. *Circulation* 85: 606–611, 1992.
21. **Parikh SM, Diedrich A, Biaggioni I, and Robertson D.** The nature of the autonomic dysfunction in multiple system atrophy. *J Neurol Sci* 200: 1–10, 2002.
22. **Robertson D.** Diagnosis and management of baroreflex failure. *Primary Cardiol* 21: 37–40, 1995.
23. **Sato T, Kawada T, Inagaki M, Shishido T, Takaki H, Sugimachi M, and Sunagawa K.** New analytic framework for understanding sympathetic baroreflex control of arterial pressure. *Am J Physiol Heart Circ Physiol* 276: H2251–H2261, 1999.
24. **Sato T, Kawada T, Shishido T, Sugimachi M, Alexander J Jr, and Sunagawa K.** Novel therapeutic strategy against central baroreflex failure: a bionic baroreflex system. *Circulation* 100: 299–304, 1999.
25. **Sato T, Kawada T, Inagaki M, Shishido T, Sugimachi M, and Sunagawa K.** Dynamics of sympathetic baroreflex control of arterial pressure in rats. *Am J Physiol Regul Integr Comp Physiol* 285: R262–R270, 2003.
26. **Sato T, Kawada T, Sugimachi M, and Sunagawa K.** Bionic technology revitalizes native baroreflex function in rats with baroreflex failure. *Circulation* 106: 730–734, 2002.
27. **Schramm LP and Livingston RH.** Inhibition of renal nerve sympathetic activity by spinal stimulation in rat. *Am J Physiol Regul Integr Comp Physiol* 252: R514–R525, 1987.
28. **Shannon JR, Diedrich A, Biaggioni I, Tank J, Robertson RM, Robertson D, and Jordan J.** Water drinking as a treatment for orthostatic syndromes. *Am J Med* 112: 355–360, 2002.
29. **Shimoji K, Hokari T, Kano T, Tomita M, Kimura R, Watanabe S, Endoh H, Fukuda S, Fujiwara N, and Aida S.** Management of intractable pain with percutaneous epidural spinal cord stimulation: differences in pain-relieving effects among diseases and sites of pain. *Anesth Analg* 77: 110–116, 1993.
30. **Shy M and Drager GA.** A neurological syndrome associated with orthostatic hypotension: a clinico-pathologic study. *Arch Neurol* 2: 511–527, 1960.
31. **Sugimachi M, Imaizumi T, Sunagawa K, Hirooka Y, Todaka K, Takeshita A, and Nakamura M.** A new method to identify dynamic transduction properties of aortic baroreceptors. *Am J Physiol Heart Circ Physiol* 258: H887–H895, 1990.
32. **Taylor RF and Schramm LP.** Spinally mediated inhibition of abdominal and lumbar sympathetic activities. *Am J Physiol Regul Integr Comp Physiol* 254: R655–R658, 1988.
33. **Wilcox CS, Puritz R, Lightman SL, Bannister R, and Aminoff MJ.** Plasma volume regulation in patients with progressive autonomic failure during changes in salt intake or posture. *J Lab Clin Med* 104: 331–339, 1984.

Diagnostic Value of the Recovery Time-Course of ST Slope on Exercise ECG in Discriminating False- From True-Positive ST-Segment Depressions

Satoru Sakuragi, MD; Hiroshi Takaki, MD; Atsushi Taguchi, MD; Kazuhiro Suyama, MD; Takashi Kurita, MD; Wataru Shimizu, MD; Toru Kawada, MD; Yoshio Ishida, MD; Tohru Ohe, MD; Kenji Sunagawa, MD

Circulation Journal
Vol. 68 No. 10 October 2004
(Pages 915–922)

Circ J 2004; **68:** 915–922

Diagnostic Value of the Recovery Time-Course of ST Slope on Exercise ECG in Discriminating False- From True-Positive ST-Segment Depressions

Satoru Sakuragi, MD; Hiroshi Takaki, MD*; Atsushi Taguchi, MD; Kazuhiro Suyama, MD; Takashi Kurita, MD; Wataru Shimizu, MD; Toru Kawada, MD*; Yoshio Ishida, MD**; Tohru Ohe, MD†; Kenji Sunagawa, MD*

Background Using the exercise ECG for diagnosing coronary artery disease (CAD) is hampered by the occurrence of false-positive (FP) ST-segment depression. Because it is known that the recovery ST-T time-course in CAD differs from that in FP subjects, the ST slope may help discriminate FP from true-positive (TP) results.
Methods and Results Treadmill digitized ECG from patients with significant ST-segment depressions and normal resting ECG were analyzed in 134 patients with CAD on angiography (>50% narrowing) and reversible perfusion defects (TP group), and 64 subjects with normal perfusion (FP group) on exercise single photon emission computed tomography. The ST slope between the J-point and J80 was measured every minute up to 6-min postexercise. The ST slope was significantly higher in FP than in TP at peak exercise, and at postexercise 1-, 2- and 3-min ($p<0.01$, all). Thereafter, it gradually increased in TP, while monotonically decreasing in FP. Its decrease from 3- to 6-min could correctly diagnose 88% of FP subjects, whereas it was found in only 19% of TP patients (total accuracy 83%).
Conclusions The ST slope change from early to late recovery is a simple yet reliable marker for discriminating FP from TP ST-segment responses in subjects with a normal resting ECG. (*Circ J* 2004; **68:** 915–922)

Key Words: Coronary disease; Electrocardiography; Exercise; Ischemia

Gender and several anatomical and functional characteristics are associated with an increased incidence of abnormal ST-segment responses to exercise in the absence of coronary artery disease (CAD). Subsets with an increased incidence of false-positive (FP) exercise ECG responses with respect to ischemia include middle-aged women[1–3] and patients with mitral valve prolapse[1,4,5] Patients with left ventricular hypertrophy (LVH) form a separate subset with the potential for inadequate myocardial perfusion in the absence of significant CAD[4,6] Advanced ECG analysis approaches applicable to the clinical evaluation of the standard exercise ECG in these subjects are currently unavailable and need to be developed.

The ST slope, usually computed as the slope between the J-point and the J80, has been mainly used for differentiating the configuration of ST-segment depression (ie, upsloping, horizontal, and downsloping). The latter two are considered more specific for myocardial ischemia than the upsloping shape[1,7] However, in CAD, the shape often changes with time during the test and a relatively characteristic time-course can be seen. ST-segment depression during exercise changes from upsloping (or horizontal) to downsloping in the early recovery at 2–4 min; that is, the ST slope decreases in early recovery (Fig 1A)[7,8] Subsequently, both ST-segment depression and the ST slope return gradually toward the baseline; that is, the ST slope increases in late recovery. On the other hand, in many subjects with FP ST-segment depression (FPD) (Fig 1B), the downsloping shape appears, not in the early, but in the late recovery. Unlike in CAD, the ST slope monotonically decreases from early to late recovery, possibly serving as the differentiating characteristic[5,8]

We thus hypothesized that the temporal changes in the ST slope from early to late recovery are capable of differentiating these 2 groups and we performed high-resolution computer analysis of the ST slope in the recovery in a relatively large population with normal resting ECGs. Because the majority of subjects with normal exercise single-photon emission computed tomography (SPECT) results are no longer referred for coronary angiography in the clinical practice, we used this technique for the selection of FPD subjects. True-positive (TP) results were defined when both angiographic and exercise SPECT images were abnormal.

Methods

Study Population

From the digitized ECG recordings consecutively obtained during routine treadmill testing for the evaluation of CAD, 198 patients (62±9 years) with an exercise-induced significant ST-segment depression were recruited. Patients were excluded if they had resting ECG abnor-

(Received February 3, 2004; revised manuscript received July 7, 2004; accepted July 13, 2004)
*Division of Cardiology, Department of Medicine, National Cardiovascular Center, *Department of Cardiovascular Dynamics, National Cardiovascular Center Research Institute, **Department of Radiology and Nuclear Medicine, National Cardiovascular Center, Suita and †Department of Cardiovascular Medicine, Okayama University Graduate School of Medical and Dentistry, Okayama, Japan*
Mailing address: Hiroshi Takaki, MD. Department of Cardiovascular Dynamics, National Cardiovascular Center Research Institute, 5-7-1 Fujishiro-dai, Suita 565-8565, Japan. E-mail: htakaki@res.ncvc.go.jp

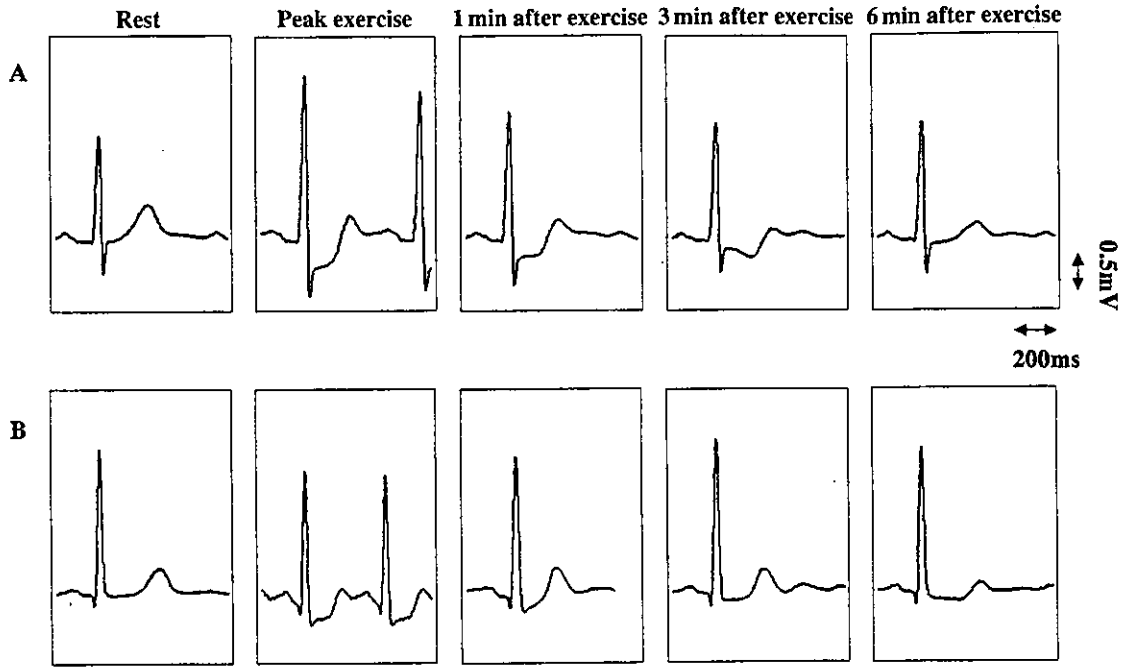

Fig 1. Representative exercise ECG from a patient with (A) true-positive (TP: V5) and (B) false-positive (FP: V6) ST-segment response. In the patient with a TP response, slow-rising ST-segment depression at peak exercise and at 1 min after exercise became downsloping at 3 min followed by its recovery at 6 min. That is, the ST slope transiently decreased soon after exercise but increased with time in late recovery. In the subject with a FP response, a horizontal ST-segment depression at postexercise 3 min became downsloping at 6 min; that is, the ST slope decreased in this late recovery.

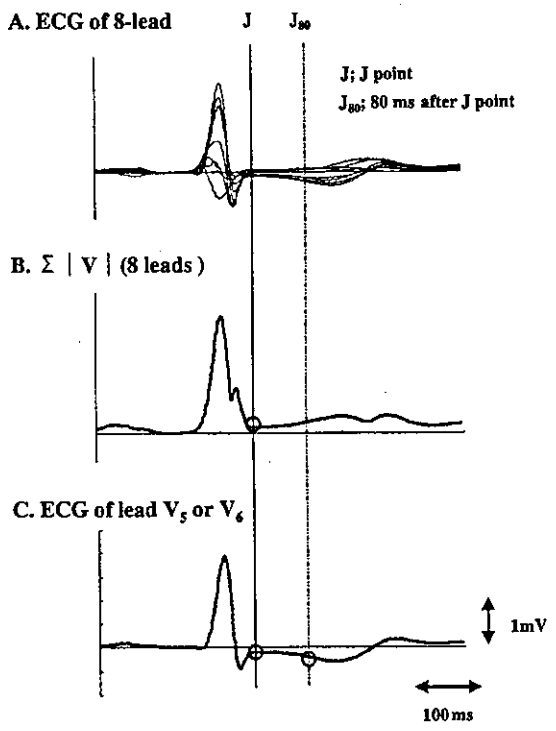

Fig 2. Computer measurements of the ST slope. From ECG data for all 8 leads (A), we computed the algebraic sum (Σ|V|) of the absolute value of voltage relative to the isoelectric Q-Q baseline (B), which was used to determine the J-point. Once the J-point was determined, ST-segment displacements from the isoelectric Q-Q baseline at the J-point and at J80 were measured automatically (C). The ST slope is derived as the slope connecting these 2 points. Vertical solid and broken lines indicate the J-point and J80, respectively.

malities such as prior myocardial infarction, ST-segment depression, T-wave inversion, LVH, or bundle branch block. We also excluded patients with atrial fibrillation or frequent extrasystole (>10 beats/min) and those with exercise-induced ST-segment elevation (≥0.1 mV). All subjects gave informed consent.

Patients were divided into the 2 groups according to the results of coronary angiography and exercise SPECT performed within 3 months after treadmill testing. The TP group comprised 134 patients (62±9 years) who had angiographical coronary artery stenosis (>50% luminal narrowing). Inducible ischemia was confirmed by the presence of reversible defects corresponding to coronary lesions. The FP group included 64 subjects (63±10 years) with normal exercise SPECT images. Of them, 19 (30%) had undergone coronary angiography and none had significant CAD.

We investigated the presence of a history of hypertension, which may be associated with a high incidence of FPD in patients with mild LVH only discernible by echocardiographic study[9,10]

Treadmill Exercise ECG

Exercise testing was performed according to our protocol, which was similar to the modified Bruce protocol[11] We performed the test using a treadmill system (Formula, Esaote, Italy), while simultaneously digitizing the ECG data at 500 Hz (12-bit resolution) from rest, during exercise, and into recovery for at least 6 min. A hard copy of the standard 12-lead ECG at a paper speed of 25 mm/s at rest, at the end of each stage, at peak exercise, and every minute into recovery was produced. Termination of exercise was decided by the occurrence of exhaustion, ST-segment depression >0.3 mV, significant arrhythmias, moderately severe angina, inadequate blood pressure response, or the attainment of 90% predicted maximal heart rate.

Table 1 Clinical Characteristics of the Study Population

	FP (n=64)	TP (n=134)
M/F (n, %)	34/30 (53/47)	118/16 (88/12)**
Age (years)	63±10	62±9
Coronary risk factors		
Hypertension (%)	44	60*
Diabetes mellitus (%)	14	40*
Medications		
Nitrates (%)	11	60**
β-blockers (%)	16	57**
Calcium-antagonists (%)	27	68**
Coronary artery disease		
LMT (%)	–	1
SVD (%)	–	46
DVD (%)	–	33
TVD (%)	–	20

*Values are mean±SD or numbers (percentage). **p<0.01 vs FP group. *p<0.05 vs FP group. FP, fales-positive; TP, true-positive; LMT, left main trunk disease; SVD, single vessel disease; DVD, double vessel disease; TVD, triple vessel disease.*

On the ECG hard copies, we identified a significant ST-segment depression according to the following criteria: (1) horizontal or downsloping ST-segment displacement at the J-point ≥0.1 mV; and (2) upsloping ST-segment displacement at J_{80} ≥0.15 mV in at least 3 consecutive beats at peak exercise. Arterial blood pressure was measured by a sphygmomanometer at the end of each stage, peak exercise and recovery.

ECG Analysis

For the standard 12-lead ECG, only 2 of 6 limb leads are actually recorded, and the other 4 leads are derived mathematically from these 2 leads.[12] Our stress system capable of reproducing the 12-lead ECG actually records 2 unique limb leads (leads I and II) and 6 precordial leads in a similar manner. We performed the following analysis using the digitized ECG data set of 8 leads (I, II, and V_{1-6}; Fig 2A).

To determine the ST slope, we found the peak of each R wave in lead V_5, with which the QRS-T complex was averaged over 5 beats to improve the signal-to-noise ratio. On the QRS-T complex, we measured ST-segment displacement at peak exercise and at every minute during the first 6 min postexercise, in a lead with a greater ST-segment depression at peak exercise of either lead V_5 or V_6. Because the J-point determination is occasionally difficult, we derived the algebraic sum ($\Sigma|V|$) of the absolute value of voltage relative to the isoelectric Q-Q baseline from all 8 leads (Fig 2B). With reference to this curve, we determined the J-point by detecting the point at which the curve most closely approached the baseline (the lowest point of the trough). If the curve did not have a distinct trough, the J-point was assumed to be the inflection point at which a steep descent of the curve was terminated. Once the J-point was determined, ST-segment displacement from the Q-Q baseline at the J-point and J_{80} was measured automatically (Fig 2C). From these 2 values, we calculated the ST slope (mV/s). The ST slope, treated as a continuous variable ranging from negative to positive values, was used for the later intra- and intergroup comparisons. The time-courses of ST-segment depression and ST slope from peak exercise to the 6-min recovery (every minute, 7 time points) were assessed.

Table 2 Exercise Test Results

	FP (n=64)	TP (n=134)	p value
Rest HR (beats/min)	72±11	67±11	<0.01
Rest SBP (mmHg)	139±22	132±19	<0.05
Peak HR (beats/min)	149±19	127±21	<0.01
Peak SBP (mmHg)	178±27	160±24	<0.01
Exercise time (s)	526±150	480±136	<0.05
Exercise-induced chest pain (%)	9	46	<0.01
ST-segment depression (mV)	–0.20±0.11	–0.22±0.12	<0.01

FP, fales-positive; TP, true-positive; HR, heart rate; SBP, systolic blood pressure.

Exercise Thallium-201 Scintigraphy

All subjects underwent bicycle exercise testing according to the same end points as defined earlier. At near-maximal exercise, thallium-201 was intravenously injected and the patient was encouraged to exercise for another 1 min. SPECT images were obtained at 15 min (initial images) and 4 h (delayed images). The images were reconstructed into transaxial tomograms, which were assessed by 2 experienced physicians unaware of the coronary anatomy. Thallium uptake in myocardial segments was classified as normal, mildly, moderately or severely reduced, or absent. A reversible defect was defined when the classification of uptake improved by at least one category from the initial to the delayed image.

Statistical Analysis

All data are presented as mean±SD. Unpaired t-test was used for comparisons between 2 groups. Differences in categorical variables were analyzed by chi-square analysis. The time-course of ST-segment depression and the ST slope were compared by analysis of variance for repeated measurement. When this test was significant, the Newman-Keuls post-hoc multiple comparison was performed.

For convenience in presentation, the term 'sensitivity' is used to measure the percentage of subjects who met the criteria for identifying FP results in the FP group. The term 'specificity' is used to measure the percentage of subjects who did not fulfill the criteria in the TP group.

Performance of diagnostic criteria was evaluated using receiver operating characteristic (ROC) curve analysis.[13,14] The area under the curve (AUC), which is a measure of the discriminatory power of the index, was calculated for each variable and these areas were compared statistically.[15] A p-value <0.05 was considered significant.

Results

Patient Characteristics

Although age was similar between the groups, the FP group included more females than the TP group (p<0.01, Table 1). Hypertension, common to both groups, was found more frequently in the TP (60%) group than in the FP group (44%, p<0.05). Approximately half of the TP patients (46%) had single-vessel disease.

Treadmill Exercise Test

Resting heart rate and systolic blood pressure were higher in the FP group than in the TP group (p<0.01 and p<0.05, respectively; Table 2). Exercise time, peak heart rate and peak systolic blood pressure were also higher in the FP group (p<0.05, p<0.01, and p<0.01, respectively). Chest

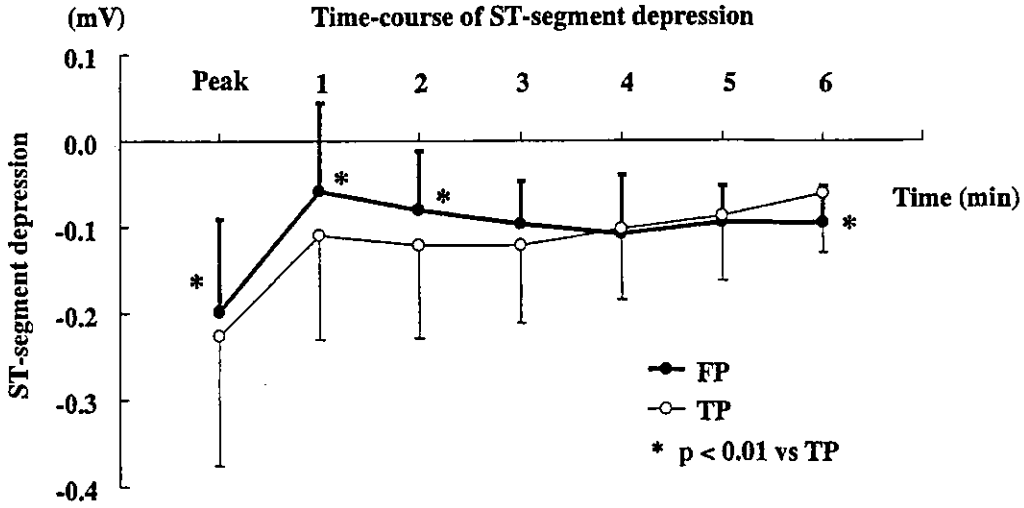

Fig 3. Comparison of the recovery time-course of ST-segment depression changes at the J80 between the false-positive (FP: closed circle) and true-positive (TP: open circle) groups. *p<0.01 vs TP.

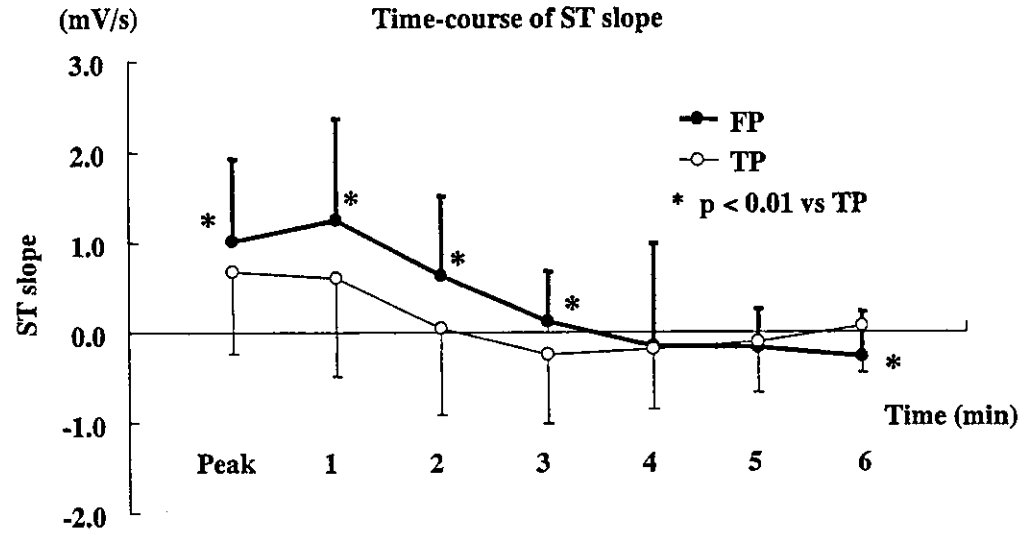

Fig 4. Comparison of the recovery time-course of changes in the ST slope between the false-positive (FP: closed circle) and true-positive (TP: open circle) groups. *p<0.01 vs TP.

pain, including atypical, equivocal, or typical features for angina, occurred in 46% of the TP group and 9% of the FP group (p<0.01) during the test. Maximal ST-segment depression (J80) was marginally but significantly greater in the TP (–0.23±0.15 mV) than in the FP group (–0.20± 0.11 mV, p=0.002, unpaired t-test).

Time-Course of ST-Segment Depression

Fig 3 shows the time-course of the recovery of ST-segment depression (J80). At peak exercise and in early recovery (at 1 and 2 min), ST-segment depression was significantly greater in the TP group (p<0.01, all) than in the FP group. No difference was observed at 3, 4, and 5 min. In the late recovery, ST-segment depression gradually recovered toward the baseline in the TP group, but remained unchanged in the FP group. Consequently, it was greater in the FP group than in the TP group at 6 min postexercise (p<0.01). Despite these differences, ST-segment depression at any time point hardly differed between the 2 groups because of a considerable overlap, evidenced by the large standard deviation.

Time-Course of the ST Slope

Fig 4 shows the time-course of the recovery of the ST slope. It decreased with time up to 3 min postexercise in each group. During this period, the ST slope was significantly lower in the TP group than in the FP group (all p<0.01). Thereafter it continued to decrease in the FP group, whereas it gradually recovered toward the baseline in the TP group. Thus, in the late recovery, the ST slope in the FP group changed in the opposite direction to that in the TP group.

Fig 5 shows the changes in the ST slope for each subject. In the FP group, the ST slope decreased between 3 and 6 min (0.12±0.55 to –0.28±0.50 mV/s, p<0.001), whereas it increased in the TP group (–0.25±0.77 to 0.06±0.52 mV/s, p<0.001). Most FP subjects (56/64, 88%) showed a decrease during this period, which was observed in only 19% of TP patients (25/134).

The time-course difference in the ST slope (ΔST Slope,

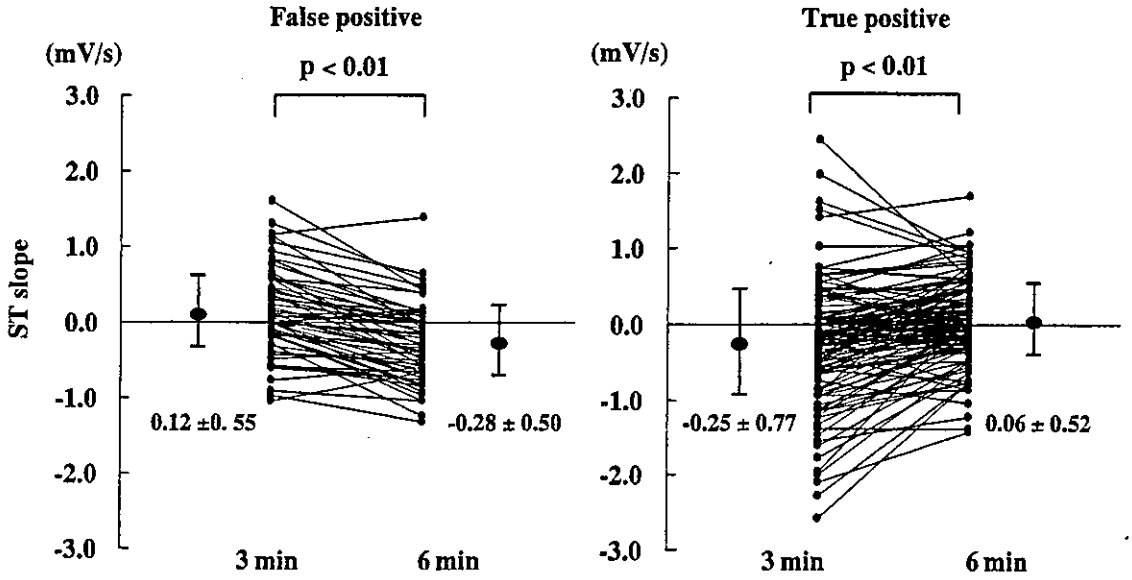

Fig 5. Changes in ST slope from 3 to 6 min after exercise in the false-positive (FP: Left) and true-positive (TP: Right) groups. Large closed circles and vertical lines represent means and 1 SD, respectively.

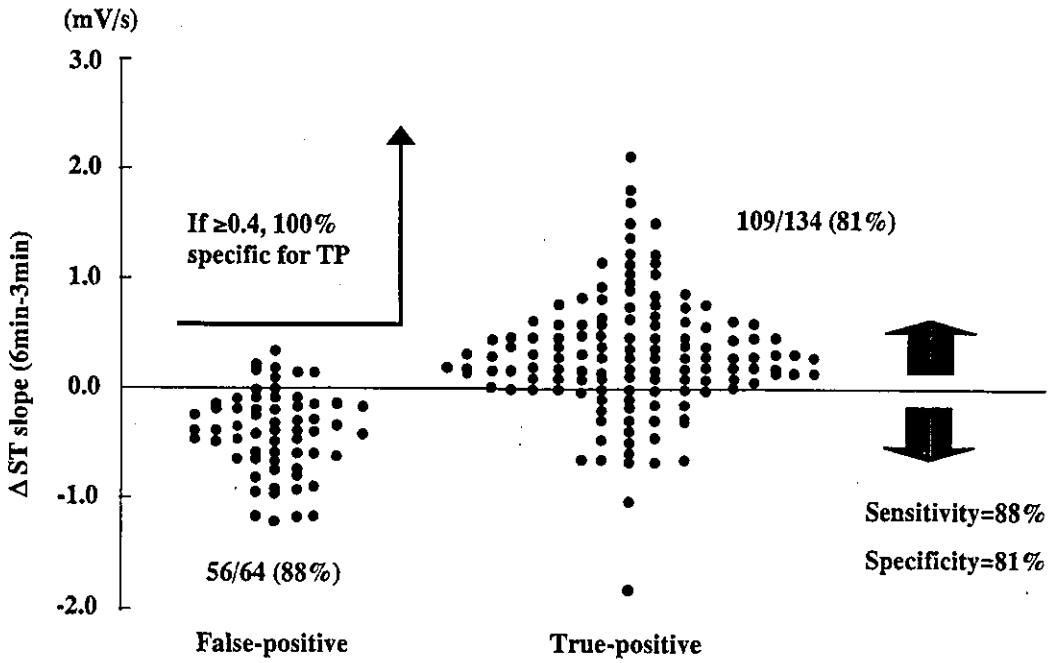

Fig 6. ΔST slope (ST slope at 6 min minus that at 3 min) is plotted for each subject in the false-positive (FP: Left) and true-positive (TP: Right) groups.

ST slope at 6 min minus that at 3 min) is plotted for each subject in Fig 6. When a decrease in the ST slope (ΔST Slope <0 mV/s) was set as the criterion for FPD, we could discriminate FP from TP patients with a sensitivity of 88% and a specificity of 81%. Conversely, its increase was highly predictive for TP patients; ΔST slope ≥0.4 mV/s was 100% predictive for TP patients (FP n=0, TP n=49) and ΔST slope ≥0.0 mV/s was 93% predictive for TP patients (FP n=8, TP n=109).

Because coronary angiography was not performed in 70% of the FP group, we performed separate subgroup analysis of subjects with (n=19) and without (n=44) angiography. As a result, the ST slope significantly decreased from postexercise 3- to 6-min in each group ($p<0.001$, for both groups). ΔST slope was very similar between the 2 groups (–0.36±0.43 mV/s with vs –0.42±0.35 mV/s without angiography, NS).

Comparison of Test Performance by ROC

Fig 7 shows the ROC curves describing the ability for the discrimination using the ST slope for 1, 3 and 6 min after exercise and ΔST slope. The AUC for ΔST slope was significantly greater than that of the ST slope obtained at any of the 3 time points ($p<0.01$, all).